Two–bump solutions of Amari–type models of neuronal pattern formation

Carlo R. Laing [a,*] and William C. Troy [b]

[a] *Institute of Information and Mathematical Sciences, Massey University, Auckland, New Zealand*

[b] *Department of Mathematics, University of Pittsburgh, Pittsburgh, PA 15260, USA.*

Abstract

We study a partial integro-differential equation defined on a spatially extended domain that arises in the modeling of pattern formation in neuronal networks. For a one–dimensional domain we develop criteria for the existence and stability of equal width "two–bump" solutions under the assumption that the firing rate function is the Heaviside function. We apply these criteria to an example for which the connectivity is of lateral inhibition type (i.e. the coupling function has one positive zero) and find that families of 2–bump solutions exist, but none of the solutions are stable. Extensive numerical searches suggest that this is true for all coupling functions of this form. However, for a large class of coupling functions which have three positive zeros, we find the coexistence of both stable and unstable 2–bump solutions. We also extend our investigation to two spatial dimensions and give numerical evidence for the coexistence of 1–bump and 2–bump solutions. Our results imply that lateral inhibition type coupling is not sufficient to produce stable patterns that are more complex than single isolated patches of high activity.

Key words: Pattern formation, integro–differential equation, short term memory, neuroscience.
PACS: 87.19.La, 89.75.Kd, 02.30.Rz

* Corresponding author. ph: +64-9-443 9799 extn. 9567, fax: +64-9-443 8181.
Email addresses: c.r.laing@massey.ac.nz (Carlo R. Laing), troy@math.pitt.edu (William C. Troy).

Preprint to appear in Physica D *21 January 2003*

1 Introduction

Pattern formation in neuronal networks is an area of ongoing interest [6,7,11,12,14,17,18,30]. In this paper we investigate spatially localized regions of high activity, often referred to as "bumps". These are of interest in modeling working memory, the ability to remember information over a time–scale of a few seconds [8,10,17,29]. Experiments on primates show that there exist neurons that have elevated firing rates during the period that the animal is "remembering" some aspect of an object or event [2,22,24]. These neurons are spatially localized in a location determined by the relevant aspect of the object or event being remembered. Other possible applications of the models investigated here include the head–direction system [26,32], feature selectivity in the visual cortex [6,7,15], the behaviour of infants repeatedly reaching towards objects [28], and robot navigation [12]. "Spiking" neuron models have been used to model bumps [8,14,17], as have "rate" models [1,16,28,31].

In this paper we extend the 1977 work of Amari [1] who found *single* spatially localized regions of high activity (bumps) in rate models of the form

$$\frac{\partial u(x,t)}{\partial t} = -u(x,t) + \int_{-\infty}^{\infty} w(x-y) f(u(y,t))\, dy + s(x,t) + h. \tag{1.1}$$

Equation (1.1) models a single layer of neurons. The function $u(x,t)$ denotes the "synaptic drive" or "synaptic input" to a neural element at position $x \in (-\infty, \infty)$ and time $t \geq 0$. The connection, or coupling, function $w(x)$ determines the coupling between elements, and the nonnegative function $f(u)$ gives the firing rate, or activity, of a neuron with input u. Neurons at a point x are said to be active if $f(u(x,t)) > 0$. The function $s(x,t)$ represents a variable external stimulus, and the parameter h denotes a *constant* external stimulus applied uniformly to the entire neural field.

In Ref. [1] Amari investigates the dynamics of pattern formation in equation (1.1) when $w(x)$ has a "mexican hat" shape corresponding to the basic coupling known as lateral inhibition (see Figure A.1). The defining feature of this type of coupling is that $w(x)$ is a continuous function which is positive at $x = 0$, and changes sign exactly once on the interval $(0, \infty)$, so that $w(x) < 0$ for large enough x. Amari also assumes that the firing function $f(u)$ is the Heaviside step function. Under the further simplifying assumption that $s(x,t) = 0$, i.e. that there is no external stimulus, Amari studies the existence and stability properties of stationary solutions of (1.1), which are solutions of

$$u(x) = \int_{-\infty}^{\infty} w(x-y) f(u(y))\, dy + h. \tag{1.2}$$

The region of excitation of a solution of (1.2) is the set

$$R(u) = \{x | u(x) > 0\}. \tag{1.3}$$

A solution for which $R(u)$ is a bounded, connected, open interval is defined to be a 1–bump solution. Amari proves that, depending on the value of h, equation (1.2) has zero, one or two 1–bump solutions. He also develops a stability criterion which shows that when two 1–bump solutions coexist (see Figure A.3), then the "larger" of these is a stable solution of the original equation (1.1), and the "smaller" solution is unstable. If, for a solution of (1.2), $R(u)$ consists of N disjoint, finite, connected, open intervals, the solution $u(x)$ is called an N–bump solution.

In this paper we extend the results described above and consider the general problem of how stationary N–bump solutions form when $N > 1$. In [18] we derived a set of reasonable assumptions on the functions w and f and began the study of this problem. In particular, we assumed that the coupling w had infinitely many positive zeros (i.e. w oscillated infinitely often between positive and negative values), as opposed to the single positive zero that is characteristic of lateral inhibition. For a specific example of such a coupling we found numerical evidence for the existence of several families of N-bump solutions, some of which appear to be stable. However, because neural connections in the brain cannot exist over arbitrarily large distances, it is equally important to understand how multi–bump solutions form when the coupling w has only a *finite* number of positive zeros.

Our primary goal is to understand the important features of coupling functions which lead to stable multi-bump stationary solutions. In order to gain the deepest possible insight our strategy here is to focus our attention on how 2–bump solutions form in a hierarchy of increasingly complicated models. 2–bump solutions can be thought of as the next most "complex" solutions after 1–bump solutions, and many of the ideas used to investigate their existence and stability may also be applicable to the study of multi–bump solutions. For each model we investigate the following important issues:

(i) Are there ranges of parameters for which zero, one or two 2–bump solutions exist? Do families of solutions arise or disappear via a bifurcation phenomenon as a parameter passes through a critical value? What are the qualitative properties of solutions (e.g. shape, distance between bumps, etc)?

(ii) Is there a range of parameters for which one or more 2–bump solutions exist, yet no 1–bump solution exists?

(iii) Are any of the 2–bump solutions stable? Can stable 1–bump and 2–bump solutions coexist?

In Section 2 we begin with a review of the techniques developed by Amari [1] to prove

the existence and stability of 1–bump solutions when the coupling is the basic lateral inhibition type having just one positive zero. In Sections 3 and 4 we generalize Amari's results and develop methods to prove the existence, qualitative behavior and stability of 2–bump solutions. We then apply these results to the lateral inhibition case and find that there is a range of parameters over which families of 2–bump solutions do exist. However, our analytical and numerical analyses indicate that these solutions are all unstable. These results suggest that to obtain stable multi–bump solutions, the coupling function should have more than one zero in $(0, \infty)$. Thus, in Section 5 we consider a simple extension to the class of couplings which have exactly three positive zeros, so that $w(x)$ is alternately positive, negative, positive and finally negative as x increases from 0 to infinity. Surprisingly, we now find that there is a range of parameters where *stable* 2–bump solutions exist, together with stable 1–bump solutions. In Section 6 we extend the model to two spatial dimensions and give numerical examples of 1–bump and 2–bump solutions for specific examples of the couplings described above. In the final section we summarize our results and discuss directions for future study of the more general problem of N–bump formation when $N > 1$.

Our motivation for choosing a coupling function with more than one positive zero is that this may better represent the connectivity known to exist in the prefrontal cortex, where studies have shown that coupled groups of neurons lie on an approximate lattice [3,13,19–21]. These connections are purely excitatory [6], and the positive sections of the coupling function $w(x)$ can be associated with them. There are also known to be inhibitory connections which have a wider extent than the local excitatory ones [25], and by adding their effect to the effect of the excitatory coupling, a coupling function with alternating positive and negative sections, as presented in Section 5, can be obtained. This form of connectivity is thus a "bridge" between the lateral inhibition used by previous authors [1,15,17] and the coupling with infinitely many zeros introduced in [18], and by studying it we hope to understand better the essential ingredients required for multi–bump solutions of equations of the form (1.1).

Other authors have also considered connectivity functions that incorporate the "patchy" nature of neural connections. Bressloff [5] recently investigated a two–dimensional system for which the connectivity function was the sum of two functions, one representing local connections, of a Mexican–hat type, and the other representing the longer–range connections, which had the form of a weakly–decaying modulation of a non–negative periodic function. By adding these two functions together, one can obtain a weakly–decaying modulation of an approximately periodic function, with both positive and negative connectivities, similar to both the family of functions presented in [18] and to the function presented in Section 5. Bressloff et al. [6,7] have also studied models for visual cortex in which both local connectivity and patchy longer–range connectivities are incorporated. They assumed that the patches were located on a precise lattice, and used group–theoretic ideas to determine the possible bifurcations from the

homogeneous state. The bifurcating solutions were then related to geometric patterns commonly observed during hallucinations.

Of course, there are a number of other simplifications involved in a model of the form (1.1). One is that the behavior of neurons can be characterized by their firing rate alone, and more importantly, that a population of both excitatory and inibitory neurons can be represented by a single population with a connectivity function that takes both positive and negative values. Ermentrout [11] showed that, provided the inhibition acts "quickly", this can be done. A more realistic approach would involve two variables, representing the activities of the excitatory and inhibitory populations, and coupling functions between and within the populations that were non–negative. Our model is less realistic in the sense that we only use one population, lumping the excitatory and inhibitory neurons together, but has the advantage of involving only one variable.

Note that we are not addressing the processes involved in the formation of the connectivities represented by $w(x)$, but are instead interested in the possible patterns of neural activity that can exist in the system once these connectivities are in place.

2 The Model

In this section we review the techniques developed by Amari [1] to analyze the formation of 1–bump solutions of (1.1) when the coupling is the simple lateral inhibition type. First, in [1,18] it is assumed that the coupling function $w(x)$ satisfies the following:

(H_1) $w(x)$ is symmetric, i.e. $w(-x) = w(x)$ for all $x \in \mathbf{R}$;
(H_2) $w(x) > 0$ on an interval $(-\bar{x}, \bar{x})$, and $w(-\bar{x}) = w(\bar{x}) = 0$;
(H_3) $w(x)$ is decreasing on $(0, \bar{x}]$;
(H_4) $w < 0$ on $(-\infty, -\bar{x}) \cup (\bar{x}, \infty)$.
(H_5) w is continuous on $\mathbf{R}$, and $\int_{-\infty}^{\infty} w(y)\, dy$ is finite.

Coupling functions satisfying (H_2) and (H_4) are representative of "lateral inhibition" [11]. That is, condition (H_2) means that nearby neural elements excite one another, however (H_4) results in an "inhibitory effect" if the distance between neural elements is greater than a certain value, $\bar{x}$. Conditions (H_1), (H_3) and (H_5) are general requirements which allow for a tractable mathematical analysis of (1.1). In order to rigorously determine the shape of steady–state solutions of (1.1), we also assume

(H_6) $w(x)$ has a unique minimum on $\mathbf{R}^+$ at a point $x_0 > \bar{x}$, and $w(x)$ is strictly increasing on (x_0, ∞).

An example of a connection function which satisfies conditions $(H_1) - (H_6)$ is

$$w(x) = Ke^{-k|x|} - Me^{-m|x|}, \tag{2.1}$$

where $K > M > 0$ and $k > m > 0$. A specific example of this "Mexican hat" type function is shown in Figure A.1 for $K = 3.5$, $M = 3$, $k = 1.8$ and $m = 1.52$. For simplicity, Amari [1] assumes that the firing rate $f(u)$ is the Heaviside step function

$$f(u) = \begin{cases} 0, \ u \leq 0 \\ \\ 1, \ u > 0 \end{cases} \tag{2.2}$$

The interpretation of (2.2) is that a neuron fires at its maximum rate when the input exceeds the threshold value $u = 0$, and does not fire otherwise.

Under assumptions $(H_1)-(H_5)$, Amari analyzes the existence and stability of stationary solutions of (1.1) when there is no inhomogeneous external stimulus, $s(x,t)$. That is, he sets $\partial u(x,t)/\partial t = 0$ and $s(x,t) = 0$ in (1.1). This reduces (1.1) to the time independent equation

$$u(x) = \int_{-\infty}^{\infty} w(x-y) f(u(y))\, dy + h. \tag{2.3}$$

Solutions of (2.3) are called *stationary* solutions of (1.1). We note that the neural system is still subject to the constant external stimulus h applied uniformly to the entire neural field. It is easily verified that if $h \leq 0$ then the constant function $u \equiv h$ is a solution of (2.3).

Single–bump solutions: For a given distribution $u(x)$, Amari defines its region of excitation to be the set

$$R(u) = \{x | u(x) > 0\}. \tag{2.4}$$

He then defines a *localized excitation* to be a pattern $u(x)$ whose region of excitation is a *finite*, open interval, i.e. $R(u) = (a_1, a_2)$, where both a_1 and a_2 are finite. If $R(u)$ is connected we refer to the pattern as a "single–bump", or "1–bump" solution. Furthermore, because (2.3) is homogeneous, it is easily verified that $u(x-a)$ is a solution for any a whenever $u(x)$ is a solution. Thus, without loss of generality, we assume that

the region of excitation for a single–bump solution has the form

$$R(u) = (0, a). \tag{2.5}$$

Remark: If (2.3) has a solution whose region of excitation consists of $N > 1$ disjoint, finite, connected, open intervals, the solution is called an *N–bump* solution. In the next section we begin an analysis of 2–bump solutions.

In his analysis of 1–bump solutions, Amari makes use of the function

$$W(x) = \int_0^x w(y)\, dy, \tag{2.6}$$

and the related quantities

$$W_m = \max_{x>0} W(x) \quad \text{and} \quad W_\infty = \lim_{x\to\infty} W(x). \tag{2.7}$$

Conditions (H_1) and (H_5) imply that $W(x)$ is odd, and that W_∞ is finite, respectively. If (2.3) has a 1–bump solution $u(x)$ whose region of excitation is given by $R(u) = (0, a)$, then $u(x)$ satisfies

$$u(x) = \int_0^a w(x-y)\, dy + h = W(x) - W(x-a) + h. \tag{2.8}$$

At the point $x = a$, equation (2.8) reduces to

$$W(a) = -h \tag{2.9}$$

since $W(x)$ is odd and $u(0) = u(a) = 0$. In turn, Amari claims that if $a > 0$ and $h < 0$ satisfy (2.9), then

$$u(x) = W(x) - W(x-a) + h. \tag{2.10}$$

is a single–bump solution of (2.3) for which $R(u) = (0, a)$.

For a given $h \leq 0$, equation (2.9) may have zero, one or two positive solutions. The exact number is determined by the relative values of W_∞, W_m and h. In Figure A.2 we show the $W(x)$ corresponding to the Mexican hat function illustrated in Figure A.1.

In Figure A.2 we see that if $W_\infty < 0 < -h < W_m$ then there are two values, a_1 and a_2, which satisfy (2.9). Setting $a = a_1$ and $a = a_2$ in (2.10) gives the corresponding single–bump solutions of (2.3). In Figure A.3 we illustrate these two solutions for the value $h = -0.07$. Amari gives arguments that indicate that the large amplitude solution corresponding to $a = a_2$ (i.e. the leftmost solution in Figure A.3) is stable, while the rightmost, smaller amplitude solution in Figure 3 corresponding to $a = a_1$ is unstable. Furthermore, as Figure A.2 indicates, if $h = 0$ then (2.9) holds only at the positive value $a = a_2 = a_*$. Setting $a = a_*$ and $h = 0$ in (2.10), one can easily show that the resulting function is still a single–bump solution of (2.3).

We note that if (2.9) has a solution for some $a > 0$ and $h > 0$ then (2.10) implies that $u(x) > 0$ for all large x, contradicting the supposition that $R(u) = (0, a)$ is finite. Thus, single–bump solutions do not exist if $h > 0$.

Next, we make a few observations concerning the *shape* of single–bump solutions (see Figure A.3). First, we conclude from hypotheses $(H_1) - (H_4)$ and (2.10) that $u(x)$ is symmetric with respect to $x = a/2$, and that $u(x)$ is increasing on $(0, a/2)$ and decreasing on $(a/2, a)$. When we consider the additional hypotheses (H_5) and (H_6), it follows from standard analysis that the solution $u(x)$ has a unique minimum on $(0, \infty)$, and that $u(x) \to h$ from below as $x \to \infty$.

3 Two–bump solutions

In this section we begin our investigation of 2–bump solutions of the equation

$$u(x) = \int_{-\infty}^{\infty} w(x - y) f(u(y))\, dy + h. \tag{3.1}$$

Here w denotes a general coupling function, and the firing rate $f(u)$ is the Heaviside function defined in (2.2). A solution $u(x)$ is called a 2–bump solution if there are values $0 < a < b < c < \infty$ such that

$$\begin{cases} u > 0 \quad \text{on} \quad (0, a) \cup (b, c), \\ u(0) = u(a) = u(b) = u(c) = 0, \\ u < 0 \quad \text{otherwise.} \end{cases} \tag{3.2}$$

Thus, a 2–bump solution is one whose region of excitation is the union of two disjoint, finite, open intervals, i.e. $R(u) = (0, a) \cup (b, c)$. An "equal width" two–bump solution

is one for which $c - b = a$.

In Theorem 3.1 we develop a constructive method to find equal width 2–bump solutions of (3.1) for a general class of coupling functions. Following this, in Theorems 3.2 and 3.3 we consider lateral inhibition type couplings and derive fairly sharp estimates for the location of the positive zeros a, b, and c of 2–bump solutions. This will be of aid in analyzing the shape of solutions. We then apply the results of Theorems 3.1–3.3 to obtain detailed properties of families of 2–bump solutions for a specific example.

In order to proceed with the development of a necessary condition for two-bump solutions to exist, we need to make one further technical assumption on the coupling function $w(x)$.

(H_7) There is a value $x^0 > x_0$ such that $w(x)$ is concave down for all $x > x^0$.

Theorem 3.1 *Suppose that hypotheses* (H_1), (H_2), (H_3), (H_5) *and* (H_7) *hold.*

(i) *If (3.1)-(3.2) has an equal width solution for some* $0 < a < b < c < \infty$, *then*

$$2W(b) + W(a-b) - W(a+b) = 0, \tag{3.3}$$

and

$$h = W(b) - W(a) - W(a+b). \tag{3.4}$$

(ii) *There is an interval* $(0, a^*)$ *such that for each* $a \in (0, a^*)$ *there are values* $b > a$ *and* $h \in \mathrm{R}$ *for which (3.3) and (3.4) are satisfied.*

The proof of this Theorem is in the Appendix.

Remarks: Theorem 3.1 gives a necessary condition which "equal width" 2-bump solutions must satisfy. However, it does not guarantee that solutions which satisfy (3.3) are actually 2-bump solutions of the full integral equation, (3.1). For this, assuming that condition (3.3) holds, we must first show that the value of h given in (3.4) is nonpositive. From (3.1) and (3.2) it follows that

$$\lim_{x \to \pm\infty} u(x) = h. \tag{3.5}$$

If it were the case that $h > 0$, then (3.5) implies that $u(x)$ eventually becomes positive and remains positive for all large x. But this violates the requirement given in (3.2) that the region of excitation is finite. Finally, if $h \leq 0$ and (3.3) holds, then one must also show that the function

$$u(x) = \int_0^a w(x-y)\,dy + \int_b^c w(x-y)\,dy + h$$
$$= W(x) - W(x-a) + W(x-b) - W(x-c) + h \tag{3.6}$$

satisfies the conditions defined in (3.2).

Note that by using (3.6) and the oddness of W, it is easy to show that equal width 2–bump solutions are symmetric with respect to $x = (a+b)/2$.

Lateral Inhibition Couplings. We now turn our attention to the qualitative analysis of 2-bump solutions when the coupling function w is specifically of lateral inhibition type and satisfies all seven hypotheses $(H_1) - (H_7)$.

In [18] we proved the following result which gives a sharp upper bound on the width between bumps:

Theorem 3.2 *Under hypotheses $(H_1) - (H_6)$, if there is an $h \leq 0$ for which (3.1) has an equal width 2–bump solution satisfying (3.2), then the distance between bumps satisfies $b - a < x_0$.*

Note that if w had finite support (violating (H_4) and (H_6)), this theorem would not hold, as bumps sufficiently far apart would not interact and thus the pair of them would be stable (assuming that a single bump was stable).

Additional estimates for the location of the zeros of 2–bump solutions are given in the next result.

Theorem 3.3 *If (3.1) has an equal width 2-bump solution satisfying (3.2) for some $0 < a < b < c < \infty$, then*

$$b > \bar{x} \quad \text{and} \quad b - a < x_0 < c = b + a, \tag{3.7}$$

Proof: We assume that an equal width 2-bump solution exists. That is, there are values a, b and h which satisfy equations (3.3) and (3.4), and $c = b + a$. Since W is odd, equation (3.3) can be written in the form

$$W(b) - W(b-a) = W(b+a) - W(b), \tag{3.8}$$

or equivalently,

$$\int_{b-a}^{b} w(x)\,dx = \int_{b}^{b+a} w(x)\,dx. \tag{3.9}$$

If $0 < b \le \bar{x}$ then our hypotheses imply that that $w(x) > w(b) \ge 0$ for $b - a \le x < b$, and $w(x) < w(b)$ for $b < x \le b + a$. From this it follows that

$$\int_{b-a}^{b} w(x)\,dx > \int_{b}^{b+a} w(x)\,dx, \tag{3.10}$$

which contradicts (3.9). Thus it must be the case that $b > \bar{x}$. Finally, suppose that $b + a \le x_0$. Then w decreases on the entire interval $(0, b + a)$ and we again obtain the inequality in (3.10), contradicting (3.9). Therefore it must be the case that $b + a > x_0$ and (incorporating the result of Theorem 3.2) the proof is complete.

An Example. In Figure A.4 we show "equal width" 2-bump solutions of (3.1) for the specific lateral inhibition coupling defined in (2.1). The parameters used in Figures A.4 and A.5 are $K = 3.5$, $k = 1.8$, $M = 3$ and $m = 1.52$. For the leftmost solution in Figure A.4 we have $a = 1$, $b = 1.419$, $c = 2.419$ and $h = -0.028$, whereas for the solution on the right the corresponding values are $a = 0.08$, $b = 1.156$, $c = 1.236$ and $h = -0.028$. Thus, for $h = -0.028$ there are *two* two-bump solutions of (3.1). These are comparable in size to the two single–bump solutions computed in Figure A.3. We note that, in accordance with Theorem 3.2, both solutions satisfy $b - a < x_0 = 1.15$ where x_0 is the value at which $w(x)$ attains its global minimum (see Figure A.1).

In Figure A.5 we let a increase from $a = 0$ and compute the bifurcation diagrams in the (a, b) plane and the (a, h) plane, for the entire family of two–bump solutions for the functions $w(x)$ and $f(u)$ defined in (2.1)-(2.2). Our experiments show that as a increases from $a = 0$, the function $h(a)$ is continuous in a and decreases from $h = 0$ to a minimum value $h = h_* < 0$, then increases until $h = 0$ at $a \approx 1.39$. Thus, for each $h \in (h_*, 0)$, there are two two–bump solutions. For $1.39 < a < 2.83$, we can still find values b and c such that condition (3.3) is satisfied. However, the corresponding values of h defined in (3.4) are positive, so the resultant formulae for $u(x)$ given in (A.2) cannot be two–bump solutions of (3.1).

4 Stability of two-bump solutions

In this section we develop a general method to determine the stability of equal width stationary two–bump solutions. We then use the resultant stability criterion to investigate the stability of 2–bump solutions when the coupling is of lateral inhibition type.

We assume that hypotheses $(H_1), (H_2), (H_3), (H_5)$ and (H_7) hold so that the existence criteria given in Theorem 3.1 are satisfied.

We assume that $u(x,t)$ is a 2–bump solution of the time dependent equation

$$\frac{\partial u(x,t)}{\partial t} = -u(x,t) + \int_{-\infty}^{\infty} w(x-y) f(u(y,t))\, dy + h, \tag{4.1}$$

and that $(x_1(t), x_2(t))$ and $(x_3(t), x_4(t))$ are intervals, with $x_2(t) < x_3(t)$, such that

$$\begin{cases} u > 0 \quad \text{on} \quad (x_1, x_2) \cup (x_3, x_4), \\ u(x_1) = u(x_2) = u(x_3) = u(x_4) = 0, \\ u < 0 \quad \text{otherwise.} \end{cases} \tag{4.2}$$

(x_1, x_2, x_3 and x_4 are analogous to $0, a, b$ and c in Section 3, but are now assumed to be functions of time.) Substitution of (4.2) into (4.1) when f is the Heaviside function leads to

$$\begin{aligned} \frac{\partial u(x,t)}{\partial t} &= -u(x,t) + \int_{x_1}^{x_2} w(x-y)\, dy + \int_{x_3}^{x_4} w(x-y)\, dy + h \\ &= -u(x,t) + W(x-x_1) - W(x-x_2) + W(x-x_3) - W(x-x_4) + h \end{aligned} \tag{4.3}$$

Equation (4.3) will play an important role in studying the motion of the points $x_1(t)$,..,$x_4(t)$. To study their dynamics we use the same approach as Amari [1]. We differentiate $u(x_i(t), t)$ with respect to t for $i = 1, 2, 3, 4$ and obtain

$$\frac{d}{dt} u(x_i(t), t) = \frac{\partial u}{\partial x}\frac{dx_i}{dt} + \frac{\partial u}{\partial t} = 0, \qquad i = 1, 2, 3, 4 \tag{4.4}$$

where both partial derivatives are evaluated at $x = x_i$. The quantities $\partial u/\partial x|_{x_i}$ are the spatial slopes of the solution profile at the endpoints of the intervals $(x_1(t), x_2(t))$ and $(x_3(t), x_4(t))$. We assume that

$$\partial u/\partial x|_{x_1} = c_1 > 0 \quad \text{and} \quad \partial u/\partial x|_{x_4} = -c_1 < 0, \tag{4.5}$$

and

$$\partial u/\partial x|_{x_2} = -c_2 < 0 \quad \text{and} \quad \partial u/\partial x|_{x_3} = c_2 > 0, \tag{4.6}$$

where c_1 and c_2 may possibly be functions of x and t. The symmetry implicit in (4.5) and (4.6) will be true for a stationary solution of (1.1) that is reflectionally–symmetric about the point halfway between the two bumps (as was the case for the equal width bumps constructed in Section 3), so (4.5) and (4.6) are reasonable approximations if the initial profile $u(x,0)$ is similar to that of the stationary solution. Substituting (4.5)–(4.6) into (4.4), and using (4.3), we obtain

$$c_1 \frac{dx_1}{dt} = W(x_1 - x_2) - W(x_1 - x_3) + W(x_1 - x_4) - h \tag{4.7}$$

$$c_2 \frac{dx_2}{dt} = W(x_2 - x_1) + W(x_2 - x_3) - W(x_2 - x_4) + h \tag{4.8}$$

$$c_2 \frac{dx_3}{dt} = -W(x_3 - x_1) + W(x_3 - x_2) + W(x_3 - x_4) - h \tag{4.9}$$

$$c_1 \frac{dx_4}{dt} = W(x_4 - x_1) - W(x_4 - x_2) + W(x_4 - x_3) + h \tag{4.10}$$

In keeping with the notation of the previous sections, we define

$$a(t) = x_2(t) - x_1(t), \quad b(t) = x_3(t) - x_1(t) \quad \text{and} \quad c(t) = x_4(t) - x_1(t), \tag{4.11}$$

so that $a(t)$ is the width of the first bump, $b(t) - a(t) = x_3(t) - x_2(t)$ is the distance between the bumps, and $c(t) - b(t) = x_4(t) - x_3(t)$ is the width of the second bump. Our goal is to determine the behavior of $a(t), b(t)$ and $c(t)$ as $t \to \infty$. Differentiating these three functions and using (4.7)-(4.10), we obtain

$$\begin{aligned} \frac{da}{dt} &= \left(\frac{1}{c_1} + \frac{1}{c_2}\right)[W(a) + h] + \frac{1}{c_1}[W(c) - W(b)] \\ &\quad + \frac{1}{c_2}[W(c-a) - W(b-a)] \end{aligned} \tag{4.12}$$

$$\begin{aligned} \frac{db}{dt} &= \frac{1}{c_1}[W(a) - W(b) + W(c) + h] \\ &\quad + \frac{1}{c_2}[W(b-a) - W(b) - W(c-b) - h] \end{aligned} \tag{4.13}$$

$$\frac{dc}{dt} = \frac{1}{c_1}[2W(c) + W(c-b) - W(c-a) + W(a) - W(b) + 2h] \tag{4.14}$$

Since we are considering "equal width" solutions, we write

$$c(t) = a(t) + b(t) \quad \forall t > 0. \tag{4.15}$$

Thus we are restricting the dynamics to the symmetric subspace in which the bumps have equal width. Condition (4.15) simplifies (4.12)-(4.14), and we obtain

$$\frac{da}{dt} = \left(\frac{1}{c_1} + \frac{1}{c_2}\right)[W(a) + W(a+b) - W(b) + h] + \frac{1}{c_2}[2W(b) - W(a+b) + W(a-b)] \tag{4.16}$$

$$\frac{db}{dt} = \frac{1}{c_1}[W(a) - W(b) + W(a+b) + h] + \frac{1}{c_2}[W(b-a) - W(b) - W(a) - h] \tag{4.17}$$

We define F and G to be the right hand sides of (4.16) and (4.17), respectively. We also assume that our two–bump stationary solution has the form given in (3.6) where $a = \bar{a}$, $b = \bar{b}$ and $c = \bar{a} + \bar{b}$, and $\bar{a}$ and $\bar{b}$ are stationary solutions of (4.16)-(4.17). These constants must satisfy the necessary conditions given in (3.3) and (3.4). Next, we linearize (4.16)-(4.17) around the solution $(a, b) = (\bar{a}, \bar{b})$. Thus, we replace c_1 and c_2 in (4.16)-(4.17) with the corresponding values obtained from the two–bump solution itself, and compute the Jacobian matrix J of the resultant system at $(\bar{a}, \bar{b})$:

$$J = \begin{pmatrix} F_a & F_b \\ G_a & G_b \end{pmatrix}, \tag{4.18}$$

where F_a, F_b, G_a and G_b are partial derivatives evaluated at $(\bar{a}, \bar{b})$, and are given by

$$F_a = \left(\frac{1}{c_1} + \frac{1}{c_2}\right)[w(\bar{a}) + w(\bar{a}+\bar{b})] + \frac{1}{c_2}[w(\bar{a}-\bar{b}) - w(\bar{a}+\bar{b})] \tag{4.19}$$

$$F_b = \left(\frac{1}{c_1} + \frac{1}{c_2}\right)[w(\bar{a}+\bar{b}) - w(\bar{b})] + \frac{1}{c_2}[2w(\bar{b}) - w(\bar{a}+\bar{b}) - w(\bar{a}-\bar{b})] \tag{4.20}$$

$$G_a = \frac{1}{c_1}[w(\bar{a}) + w(\bar{a}+\bar{b})] - \frac{1}{c_2}[w(\bar{b}-\bar{a}) + w(\bar{a})] \tag{4.21}$$

$$G_b = \frac{1}{c_1}[w(\bar{a}+\bar{b}) - w(\bar{b})] + \frac{1}{c_2}[w(\bar{b}-\bar{a}) - w(\bar{b})] \tag{4.22}$$

The eigenvalues, λ, of J satisfy

$$\lambda^2 - (F_a + G_b)\lambda + F_a G_b - F_b G_a = 0. \tag{4.23}$$

If both eigenvalues have negative real parts then $(a, b) = (\bar{a}, \bar{b})$ is a stable solution with respect to perturbations within the symmetric subspace. If at least one eigenvalue has positive real part then $(\bar{a}, \bar{b})$ is unstable.

Lateral Inhibition Couplings. We now investigate the stability of the equal width two–bump solutions computed in Section 3 for the specific coupling function given in (2.1).

To determine the stability of these solutions, we compute the signs of the trace and determinant of the Jacobian matrix. From (4.19)–(4.22) we find that the trace is

$$F_a + G_b = \left(\frac{1}{c_1} + \frac{1}{c_2}\right)[w(a) - w(b)] + \frac{2w(a+b)}{c_1} + \frac{2w(a-b)}{c_2}, \tag{4.24}$$

and the determinant is given by

$$\begin{aligned} F_a G_b - F_b G_a = & \frac{2}{c_1 c_2}[w(a) - w(b)][w(a+b) + w(b-a)] \\ & + \frac{4}{c_1 c_2}[w(a+b)w(b-a) - w(b)w(a)], \end{aligned} \tag{4.25}$$

where we have dropped the bars from $\bar{a}$ and $\bar{b}$.

First, we consider the "small" two–bump solutions (see Figure A.4, right). These correspond to solutions with small a along the bifurcation curves given in Figure A.5. We conclude from (3.7) in Theorem 3.3 that

$$b \to x_0 \quad \text{as} \quad a \to 0^+ \tag{4.26}$$

along the bifurcation curve. Therefore, from (4.24) and (4.26) it follows that

$$F_a + G_b \to \left(\frac{1}{c_1} + \frac{1}{c_2}\right)(w(0) + w(x_0)) \quad \text{as} \quad a \to 0^+. \tag{4.27}$$

Recall from hypotheses $(H_1) - (H_7)$ that $w(x)$ is positive and symmetric, and decreases to a unique negative minimum on the interval $(0, x_0)$. Furthermore, for the parameter values we are considering it is the case (see Figure A.1) that

$$w(0) > -w(x_0). \tag{4.28}$$

This inequality, (4.27) and continuity imply that $F_a + G_b > 0$ along the bifurcation diagram when $a > 0$ is small. Since the trace of the Jacobian is the sum of the eigenvalues, it must be the case that at least one eigenvalue has positive real part when $a > 0$ is small, and therefore the corresponding two–bump solutions are unstable. Our computations, shown in Figure A.6, indicate that $F_a + G_b$ is actually negative for some

range of a values, but for these values the determinant of the Jacobian is also negative, so that at least one eigenvalue is positive, and thus all of the 2–bump (equal–width) solutions are unstable for this example. Note that since these solutions are unstable with respect to perturbations that preserve the equal–width condition, they will be unstable with respect to general perturbations.

We have computed the trace and determinant as functions of a for over 1200 randomly chosen values for $K,\ k,\ M$ and m which give lateral inhibition type coupling, and in each case we found that all 2–bump solutions are unstable. In a similar way, we studied the stability of 2–bump solutions when the lateral inhibition coupling consists of the difference of two Gaussians, namely

$$w(x) = Ke^{-kx^2} - Me^{-mx^2}. \tag{4.29}$$

For more than 1200 randomly chosen combinations of the parameters $K,\ k,\ M$ and m, we also found that all 2–bump solutions were unstable. These results strongly suggest that when the coupling is of lateral inhibition type, 2–bump solutions may exist, but they are unstable. We note, however, that a rigorous proof of instability, as well as the resolution of the general case, remain open problems. It would also be interesting to resolve the following problems:

(i) Determine stability properties of 2–bump solutions when the restriction given in (4.28) is removed.

(ii) Do the same when the firing rate function f is continuous rather than the Heaviside function. Recent results [9] suggest that doing this may allow the existence of stable 2–bump solutions when the coupling function is a difference of Gaussians, although the results in [9] are only numerical.

(iii) Extend the results of Theorem 3.2 to apply to general N–bump solutions for both finite and infinite domains.

(iv) For the interval $(-\infty, \infty)$, or for a given finite interval $(-d, d)$, extend the results of Sections 3 and 4 and find the maximum $N \geq 1$ for which stationary N–bump solutions exist. Extend the stability analysis developed above and develop criteria for both stability and instability of N–bump solutions for any $N \geq 1$.

5 A natural extension of lateral inhibition coupling

In this section we show that the multiplicity and stability of 2–bump solutions of

$$u(x) = \int_{-\infty}^{\infty} w(x-y) f(u(y))\, dy + h \tag{5.1}$$

can change when the hypotheses on w are relaxed. For simplicity we still assume that $f(u)$ is the Heaviside function, and that the basic hypotheses (H_1), (H_5) and (H_7) hold. Thus, w is continuous, symmetric and integrable on R, and concave down for large x. However, we no longer require w to have only one positive zero. Instead, we replace (H_2), (H_3), (H_4) and (H_6) with the following two hypotheses (see Figure A.7):

(H_8) $w(0) > 0$, and w has exactly three positive zeros at values $0 < s_1 < s_2 < s_3$.
(H_9) $W(s_2) > W(s_3) - W(\infty) > 0$.

Remarks: Since $W(x) = \int_0^x w(t)dt$, it follows that (H_9) can be written as

$$\int_0^{s_1} w(t)\,dt > -\int_{s_1}^{s_2} w(t)\,dt - \int_{s_3}^{\infty} w(t)\,dt. \tag{5.2}$$

This can be interpreted to say that the area under the curve $w(x)$ over $(0, s_1)$ is larger than the sum of areas between $w(x)$ and the x–axis over $(s_1, s_2) \cup (s_3, \infty)$ (see Figure A.7). We will use inequality (5.2) to determine the sign of h in equation (5.1).

Before stating our main results we recall from Theorem 3.1 that the zeros a, b, and c of an equal width 2–bump solution of (5.1) satisfy $c = a + b$, as well as the condition (3.3). The corresponding value of h is given by (3.4).

In Theorem 5.1 we keep a fixed and investigate the multiplicity and stability of 2–bump solutions when b is allowed to vary. In particular, we derive a simple criterion which guarantees that equation (3.3) has at least three solutions, one of which satisfies the criteria for stability given in Section 4. In Theorem 5.2 we show that a general class of coupling functions exists which satisfy the requirements of Theorem 5.1. After proving this result we consider a specific example and illustrate the global behaviour, including multiplicity and stability, of families of 2–bump solutions.

Theorem 5.1 *Assume that hypotheses (H_1), (H_5), (H_7), (H_8) and (H_9) hold. Suppose that $a_1 > 0$ and $b_1 > a_1$ exist such that (3.3) is satisfied when $(a, b) = (a_1, b_1)$, and that*

$$2W(a_1) - W(2a_1) > 0 \tag{5.3}$$

and

$$s_1 < a_1 < s_2 < b_1 < s_3 < c_1 = a_1 + b_1 \quad \text{and} \quad s_1 < b_1 - a_1 < s_2. \tag{5.4}$$

(i) Then there are two additional values of b, denoted by b_2 and b_3, with

$$a_1 < b_2 < b_1 < b_3, \tag{5.5}$$

such that if $(a,b) = (a_1, b_2)$ *or* $(a,b) = (a_1, b_3)$ *then equation (3.3) is satisfied.*

(ii) For each $i \in \{1,2,3\}$, *if* $(a,b) = (a_1, b_i)$ *and* h_i *is defined by (3.4), then* $h_i < 0$.

(iii) If $(a,b) = (a_1, b_1)$ *then the conditions for stability of the solution are satisfied.*

The proof of this Theorem is in the Appendix.

Remarks: In Theorem 5.2 we will show that there does exist a class of coupling functions which satisfy the requirements of Theorem 5.1. Although we construct a specific coupling function, it will be obvious that generalizations to a wider class of couplings can immediately be made.

First, we specify the values a_1, b_1 and c_1 by setting

$$a_1 = (s_1 + s_2)/2,\ b_1 = 2a_1 \ \text{ and } \ c_1 = a_1 + b_1 = 3a_1, \tag{5.6}$$

and define the four associated "areas" (see Figure A.8)

$$A_1 = -\int_{a_1}^{s_2} w(t)\,dt,\ A_2 = \int_{s_2}^{2a_1} w(t)\,dt,\ A_3 = \int_{2a_1}^{s_3} w(t)\,dt,\ A_4 = -\int_{s_3}^{3a_1} w(t)\,dt. \tag{5.7}$$

Note that $A_1, \ldots, A_4$ are all positive.

To show that a_1, b_1 and c_1 satisfy conditions (5.3) and (5.4) we make two further assumptions on the coupling function, $w(x)$:

(H_{10}) $0 < s_1 < s_3 - s_2$ and $s_3 < 3(s_1 + s_2)/2$.
(H_{11}) $A_1 = A_2$ and $A_3 = A_4$.

Hypothesis (H_{10}) gives reasonable lower and upper bounds on the positions of s_1, s_2 and s_3, and on the "width" of the region between s_2 and s_3 (see Figure A.8). Hypothesis (H_{11}) gives a relationship between the four areas A_1, A_2, A_3 and A_4. In the proof of Theorem 5.2 this relationship will play an important role in showing that conditions (3.3), (5.3) and (5.4) are satisfied. For fixed a_1, s_2 and s_3, it can be seen that an initially chosen $w(x)$ can be "tweaked" by adding appropriately chosen sufficiently differentiable functions with finite support to $w(x)$, so as to ensure that (H_{11}) is satisfied, without violating any of the other necessary hypotheses.

Theorem 5.2 *Assume that* $(H_1), (H_5)$ *and* $(H_7) - (H_{11})$ *hold, and that* $a_1,\ b_1$ *and* c_1 *are given by (5.6). Then (3.3), (5.3) and (5.4) are satisfied when* $(a,b) = (a_1, b_1)$.

The proof of this Theorem is in the Appendix.

Remarks. In Theorem 5.1 we have derived necessary conditions for the coexistence of several 2–bump solutions. In particular, our criteria guarantee the coexistence of at least three solutions of (3.3), one of which satisfies the conditions for stability. In Theorem 5.2 we constructed a class of couplings for which the criteria in Theorem 5.1 are satisfied.

An Example. We now investigate a particular example of a coupling function $w(x)$ for which there are branches of 2–bump solutions as described above in Theorems 5.1 and 5.2. Here we restrict our attention to the one–dimensional problem. In the next section the two–dimensional case will be addressed.

In one space dimension our example consists of the equation

$$\frac{\partial u(x,t)}{\partial t} = -u(x,t) + \int_{-\infty}^{\infty} w(x-y) f(u(y,t)) dy + h, \tag{5.8}$$

where $f(u) = H(u)$ (i.e. the Heaviside function), and the coupling w has the form

$$w(x) = 2e^{-k|x|}(1 - d_1 x^2 + d_2 x^4 - d_3 x^6). \tag{5.9}$$

The specific parameters are given by

$$k = 1,\ d_1 = \frac{2}{3},\ d_2 = \frac{1}{18},\ d_3 = \frac{1}{1200}. \tag{5.10}$$

Note that $w(x)$ is even and has exactly 3 positive zeros (see Figure A.9). Furthermore, hypotheses $(H_1), (H_2), (H_3), (H_5), (H_7), (H_8)$ and (H_9) are all satisfied for this function. In Figure A.9 (right) we show a blowup of the coupling function shown in Figure A.9 (left). This shows the positions of the points s_i where $w = 0$, and also the points β_i where $w' = 0$. This diagram will help illustrate the connections between our example and the existence and stability results given in Theorems 5.1 and 5.2.

1-Bump Solutions. Recall from Section 2 that the 1–bump solution given by (2.8) exists and is stable for values of a such that $W(a) \geq 0$ and $W'(a) < 0$. For lateral inhibition type couplings (i.e. $w(x)$ has one positive zero) there is exactly one interval of positive a values such that $W(a) \geq 0$ and $W'(a) < 0$ (see Figure A.2). Figure A.10 illustrates $W(a)$ for our example where the coupling is defined by (5.9)-(5.10) (Note that we have plotted $h = -W(a)$). We see that there are now *two* intervals of positive

a values (indicated by + signs on the curve) where $W(a) \geq 0$ and $W'(a) < 0$. In the general case there will always be at least two such intervals when the coupling function w has three or more positive zeros. We see that if $-0.95 < h < -0.8$ then *four* 1–bump solutions coexist, two of which are stable and two of which are unstable. Figures A.11 and A.12 shows four such solutions for $h = -0.85$.

2–Bump Soutions. In Section 3 it was shown that the region of excitation for an equal–width 2-bump stationary solution has the form $R(u) = (0, a) \cup (b, a + b)$, where $0 < a < b$.

It was also shown that a and b must satisfy (3.3) and that the corresponding value of h is given by (3.4).

We have found that for the coupling function used, for each $a > 0$ there are *three* values of b which solve (3.3). These are shown in Figure A.13. The three branches of solutions are labeled S_1, S_2 and S_3. Along each branch we determined the stability of the corresponding solution by applying the criterion developed in Section 4. We find that all solutions along S_1 and S_3 are unstable. However, on S_2 there are *two* intervals of a values (indicated by + signs in Figure A.13) where the 2–bump solutions are *stable* with respect to perturbations that do not break the equal–width condition.

Furthermore, along each S_i we see that $b(a) \to \beta_i$ as $a \to 0^+$, where β_i denotes the ith positive zero of $w'(x)$ (see Figure A.9 (right)). The estimates given in Theorem 3.3 in Section 3 show that this same phenomenon occurs for lateral inhibition couplings (see Figures A.4 and A.5). For general couplings having $N > 3$ positive zeros, we conjecture that a similar phenomenon will occur leading to N distinct families of 2–bump solutions, and possibly to other families of multi–bump solutions as well.

To show that the hypotheses of Theorem 5.1 are satisfied for a particular solution from Figure A.13, we show in Figure A.14 the stable 2–bump solution corresponding to the point $(a, b) = (2.95, 5.56) \in S_2$. The zeros of this solution (shown with a solid curve) interlace with the zeros of the coupling function $w(x)$ (dashed curve) in the correct way (inequalities (5.4)). The full graph of this solution is given in Figure A.17 (right panel). It can be shown that $2W(a) - W(2a) > 0$ for the $w(x)$ given in (5.9)-(5.10) and all a values of interest, and thus the hypotheses of Theorem 5.1 are satisfied.

Next, we compare our results for 2–bump solutions with those shown in Figure A.10 for 1–bump solutions. We compute $h(a)$ (using (3.3) and (3.4)) along each of the curves S_1, S_2 and S_3 in Figure A.13 — this is shown in Figure A.15, where the curves have been labeled Γ_1, Γ_2 and Γ_3, corresponding to S_1, S_2 and S_3, respectively. We see that $h < 0$ for all relevant values of a, for all three curves. Recall that along Γ_1 and Γ_3 the solutions are unstable. However, along Γ_2, the curve corresponding to S_2, there are two intervals where 2–bump solutions are stable.

To compare our 1–bump and 2–bump results, we have graphed in Figure A.16 both Γ_2 and Γ_0, the curve in Figure A.10 representing 1–bump solutions. We find that if $-0.875 < h < -0.8$ then four 1–bumps solutions (two stable and two unstable), and four 2–bump solutions (two stable and two unstable) coexist. For the particular choice $h = -0.85$, these eight solutions are graphed in Figures A.11, A.12, A.17 and A.18.

While we have only considered that stability of fixed points of (4.16)-(4.17), thus only taking into account perturbations that preserve the "equal bump width" condition, by directly integrating the three ODEs (4.12)-(4.14) it was found that stable fixed points of (4.16)-(4.17) can also be stable fixed points of (4.12)-(4.14) (not shown). The equations (4.12)-(4.14) do not assume that the bumps have equal width, so stable fixed points of these equations are stable to arbitrary perturbations. Proving the stability of fixed points of (4.12)-(4.14) remains a challenge for the future.

6 Extension to two space dimensions

In this section we extend our model to two spatial dimensions. This is more realistic for situations in which the position of a bump in a two–dimensional domain is of interest, e.g. if it encodes the position of an image on the retina (see, for example, Fig. 5 in [23]). Also, the cortex is an essentially two–dimensional sheet. The system we study, in analogy with (2.1)-(2.3), is the following:

$$\frac{\partial u(x,y,t)}{\partial t} = -u(x,y,t) + \iint_{\Omega} w(x-q, y-s) f(u(q,s,t))\, dq\, ds + h, \tag{6.1}$$

where Ω is an open connected subset of $\mathbf{R}^2$, $f(u)$ is the Heaviside function, and $w(x,y)$ is the coupling function. Again, we have assumed that there is no external inhomogeneous term. We will consider two particular couplings. The first is a generalization of lateral inhibition type couplings from Section 2, and the second is the generalization of the coupling with three positive zeros studied in the previous section. For each example we will compute both 1–bump and 2–bump solutions for appropriate chosen parameter values which will allow comparisons with our results for one spatial dimension.

In Figures A.19 and A.20 we have computed stable one–bump and two–bump solutions of (6.1) for the function

$$w(x,y) = Ke^{-k\sqrt{x^2+y^2}} - Me^{-m\sqrt{x^2+y^2}}. \tag{6.2}$$

The coupling function in (6.2) is the two-dimensional version of the "mexican hat" coupling given in (2.1), with distance in one dimension now replaced by distance in two dimensions. The domain Ω is a square of side–length 10, discretized by a regular 50×50 grid, with open boundaries. For both solutions the initial input for $u(x, y, 0)$ is random but localized. It remains an open problem to give a proof of existence and stability of the solutions shown in Figure A.19 and A.20.

Next, we compute 1–bump and 2–bump solutions for the coupling

$$w(x, y) = 2e^{-k\sqrt{x^2+y^2}}[1 - d_1(x^2 + y^2) + d_2(x^2 + y^2)^2 - d_3(x^2 + y^2)^3]. \tag{6.3}$$

The specific parameters are given by

$$k = 1,\ d_1 = \frac{2}{3},\ d_2 = \frac{1}{18},\ d_3 = \frac{1}{1200}. \tag{6.4}$$

This problem is the two–dimensional analogue of (5.9)-(5.10), i.e. of the model in which the coupling function has three positive zeros in one dimension, considered in the previous section.

In Figures A.21 to A.24 we show two stable 1–bump solutions, and two stable 2–bump solutions. For each of these we keep $h = -0.85$ which allows for comparisons with the analogous one-dimensional solutions shown in Figures A.11, A.12, A.17 and A.18 in the previous section. The domain was discretized with an 85 by 85 grid.

These solutions are only stable in the sense that numerical integration of the governing equations, (6.1), converges to them. (Numerical methods are described in Ref. [18].) Proof of the existence of such solutions, and in particular, the determination of their stability, remain open problems.

7 Summary

In this paper we have studied steady states of a partial integro–differential equation that has been used to model working memory in a neuronal network. Our main goal throughout the paper has been to determine the types of coupling functions for which stable 2–bump solutions exist. It is hoped that by focusing on properties of 2–bump solutions we will obtain new insights which apply to the study of N–bump solutions for any $N > 1$.

The first part of our investigation has led to the following results in one spatial dimension:

(i) the development of a general formula describing equal width 2–bump solutions;
(ii) the development of a criterion for the stability of equal width 2–bump solutions.

We applied these criteria to a wide class of randomly chosen models for which the coupling function is of lateral inhibition type and the firing rate is a step function. We found that 2–bumps solutions may exist, but if they do, they are unstable. Thus, when the firing rate is a step function, we conjecture that no stable 2–bump solutions exist for lateral inhibition type coupling.

In the second part of the paper we relax our hypotheses and investigate the class of couplings which have three positive zeros. Here we have the following results:

(iii) the development of a criterion for the existence of *three* families of 2–bump solutions;
(iv) the development of a criterion that guarantees the stability of a 2–bump solution when the zeros of the solution interlace with the zeros of the coupling function in an appropriate fashion.

We constructed a general class of couplings which have three positive zeros and which satisfy the criteria in $(iii) - (iv)$. We completely analyzed a typical example and found a range of h values in which *two* stable 1–bump solutions and *two* stable 2–bump solutions coexist. We then extended our example to include two spatial dimensions. Here we again find the coexistence of at least two stable 1–bump solutions and at least two stable 2–bump solutions. This implies that in order to obtain patterns that are more complex than a single isolated bump, a coupling function with more than one positive zero is necessary.

The possibility of the system (1.1) having more than one attractor for fixed parameter values is of interest. It would be interesting to investigate the relative sizes of the domains of attraction for the coexisting solutions, and the robustness of the system to external stimuli, e.g. noise. Competition between different attractors in a system of the form (1.1) under dynamic input has been suggested as a model for visual attention [28], and the coexistence of two attractors in a similar system has been used to model various aspects of visual perception [12]. Although we do not have an obvious interpretation for the 2–bump solutions we have investigated here, we feel that these results may be relevant in determining which possible patterns can occur in neural models that more realistically take into account the complex couplings between neurons.

There are several ways to extend the results obtained in this paper. In one spatial dimension it would be interesting to study coupling functions which have more than three positive zeros. For example, if w has five positive zeros then w' has at least five

positive zeros, $\beta_1, .., \beta_5$, and for each i we conjecture that a family of 2–bump solutions arises through a bifurcation from the point $(a, h, b) = (0, 0, \beta_i)$. This would lead to five branches of solutions similar to the three shown in Figure A.13. It should be possible to extend the methods developed here to determine the stability of solutions along these new branches. For the general case, extensions of our methods should also give new results concerning the existence, multiplicity and stability of N–bumps solutions for any $N > 1$. It would be interesting to relate results of this form to the results in Ref. [18], where families of N–bumps were investigated, although a smooth firing function f was used in that paper. Other recent relevant work is that of Coombes et al. [9] in which w retains a mexican–hat structure (i.e. lateral inhibition), but now the assumption on firing rate is relaxed and is taken to be a sigmoidal function. For a particular example they give numerical evidence that there exists a range of h over which pairs of N–bump solutions exist for every $N > 1$. For each such pair they conjecture that the one with the larger L^2 norm is stable. It is interesting to note that their assumptions give at most one stable N–bump solution for any $N > 1$, whereas our approach of modifying the coupling function results in the coexistence of two stable 1–bump solutions and two stable 2–bump solutions. A more general extension could involve combining the ideas of Bressloff [4] regarding pattern formation on inhomogeneous domains with the type of coupling function introduced here; or using one population of excitatory neurons and one of inhibitory neurons, together with appropriate non–negative coupling weights, to see if the results found here could be reproduced.

In two spatial dimensions there are very few rigorous results, although some progress has been made on circularly–symmetric solutions [27,30]. It remains a challenge to develop methods that lead to the types of non–circularly–symmetric solutions we have found, as these are at least as interesting from a biological point of view as solutions in one spatial dimension.

A Proofs

We now state some of the Theorem proofs omitted from the main text.

A.1 Proof of Theorem 3.1

We assume that there is an $h \in \mathbf{R}$ such that (3.1) has a solution satisfying (3.2). From (2.2), (3.1) and (3.2) it follows that $u(x)$ can be written as

$$u(x) = \int_0^a w(x-y)\,dy + \int_b^c w(x-y)\,dy + h \quad \forall x \in \mathbf{R}. \tag{A.1}$$

Hypotheses (H_1) and (H_5) imply that $W(x)$ is continuous and odd.

Using (2.6), we write (A.1) as

$$u(x) = W(x) - W(x-a) + W(x-b) - W(x-c) + h. \tag{A.2}$$

Because $u(a) = u(b) = u(c) = W(0) = 0$, it follows from (A.2) that

$$W(a) + W(a-b) - W(a-c) + h = 0 \tag{A.3}$$
$$W(b) - W(b-a) - W(b-c) + h = 0 \tag{A.4}$$

and

$$W(c) - W(c-a) + W(c-b) + h = 0. \tag{A.5}$$

The system (A.3)-(A.5) consists of three equations in the four unknowns. Assuming that the two bumps are of equal width, we set $c - b = a$, and (A.4)-(A.5) become

$$W(b) - W(b-a) - W(-a) + h = 0 \tag{A.6}$$

and

$$W(a+b) - W(b) + W(a) + h = 0. \tag{A.7}$$

(Using the oddness of W, we see that substituting $c-b = a$ into (A.3) gives an equation equivalent to (A.6).) A subtraction of (A.7) from (A.6) leads to

$$2W(b) + W(a-b) - W(a+b) = 0. \tag{A.8}$$

This establishes the necessary condition given in (3.3).

Next, we use (A.8) to prove part (ii). For this we find it convenient to set $b = x + a$ in (A.8) and investigate the resulting function

$$z(x) \equiv 2W(a+x) + W(-x) - W(2a+x), \quad x > 0. \tag{A.9}$$

Thus, for each a in some open interval whose left endpoint is 0, we need to show that there is a first $x_a > 0$ such that $z(x_a) = 0$. We will then set $b = a + x_a$ and $c = b + a$. The first step is to set $x = 0$ in (A.9) and investigate the resulting function

$$g(a) \equiv 2W(a) - W(2a), \quad a > 0. \tag{A.10}$$

It follows from our hypotheses that $g(a)$ is a C^1 function on $[0, +\infty)$, and that

$$g'(a) = 2[w(a) - w(2a)]. \tag{A.11}$$

It is clear that $g(0) = g'(0) = 0$. Recall that $w(0) > 0$, and that $w(x)$ decreases to zero at $x = \bar{x}$. Thus, there is a value $\bar{a} \in (0, \infty)$ such that $w(a) > w(2a)$ for $0 < a < \bar{a}$. Therefore

$$g'(a) > 0 \quad \text{and} \quad g(a) > 0 \quad \text{for} \quad 0 < a < \bar{a}. \tag{A.12}$$

From these properties it follows that there is a maximal $a^* \in (0, \infty)$ such that

$$g(a) = 2W(a) - W(2a) > 0 \quad \forall a \in (0, a^*). \tag{A.13}$$

We now keep $a \in (0, a^*)$ fixed and return to the analysis of the function $z(x)$ defined in (A.9). From (A.9) and (A.13), and the fact that W is odd, we conclude that

$$z(0) = g(a) > 0 \quad \text{and} \quad z(+\infty) = 0. \tag{A.14}$$

Furthermore, (A.9) and our hypotheses imply that $z(x)$ is continuous on $[0, +\infty)$. Next, we prove that $z(x)$ is negative for large enough x. Because $z(\infty) = 0$, it suffices to show that $z'(x) > 0$ for large x. A differentiation of (A.9) gives

$$z'(x) = 2w(a + x) - w(x) - w(2a + x), \quad x > 0. \tag{A.15}$$

Rearranging terms, we obtain

$$z'(x) = [w(a + x) - w(x)] - [w(2a + x) - w(a + x)], \quad x > 0. \tag{A.16}$$

It immediately follows from (A.16) and hypothesis (H_7) that $z'(x) > 0$ and $z(x) < 0$ for sufficiently large $x > 0$. From these properties and the continuity of $z(x)$ it follows that there is a first value $x_a > 0$ such that $z(x_a) = 0$. We then define $b = a + x_a$ and

set $c = b + a$. Finally, if there is a 2–bump solution corresponding to these values of a, b and c then it follows from the oddness of W and (A.2), and the requirement that $u(0) = 0$, that the constant h in (A.1) satisfies (3.4). This completes the proof.

A.2 Proof of Theorem 5.1

Part (i). In a similar way to that done in Theorem 3.1 we analyze the functions

$$z(x) = 2W(a_1 + x) + W(-x) - W(2a_1 + x) \tag{A.17}$$

and

$$z'(x) = 2w(a_1 + x) - w(x) - w(2a_1 + x). \tag{A.18}$$

From (5.3), (A.17) and (A.18) we obtain

$$z(0) = 2W(a_1) - W(2a_1) > 0. \tag{A.19}$$

Thus, there is an interval $(0, \delta_0)$ such that

$$z(x) > 0 \quad \forall x \in (0, \delta_0). \tag{A.20}$$

Next, we have assumed that (3.3) is satisfied when $(a, b) = (a_1, b_1)$. That is,

$$2W(b_1) + W(a_1 - b_1) - W(a_1 + b_1) = 0. \tag{A.21}$$

Also, from the requirements on a_1 and b_1 given in (5.4) it follows (see Figure A.7) that

$$w(b_1) > 0, \;\; w(b_1 - a_1) < 0 \;\; \text{and} \;\; w(a_1 + b_1) < 0. \tag{A.22}$$

We let $x_1 = b_1 - a_1$ in (A.17) and (A.18), and use (A.21) and (A.22) together with the fact that w is an even function, to obtain

$$z(x_1) = 0 \;\; \text{and} \;\; z'(x_1) = 2w(b_1) - w(b_1 - a_1) - w(a_1 + b_1) > 0. \tag{A.23}$$

Thus, there is an interval of the form $(x_1 - \delta_1, x_1 + \delta_1)$ such that

$$z(x) < 0 \quad \forall x \in (x_1 - \delta_1, x_1), \quad \text{and} \quad z(x) > 0 \quad \forall x \in (x_1, x_1 - \delta_1). \tag{A.24}$$

We conclude from (A.20), (A.24) and the continuity of $z(x)$, that there is a first $x_2 \in (0, x_1)$ such that $z(x_2) = 0$. Thus, when $x = x_2$, equation (A.17) becomes

$$2W(a_1 + x_2) + W(-x_2) - W(2a_1 + x_2) = 0. \tag{A.25}$$

We define $b_2 = a_1 + x_2$ and write (A.25) as

$$2W(b_2) + W(a_1 - b_2) - W(a_1 + b_2) = 0. \tag{A.26}$$

Thus (3.3) is satisfied when $(a, b) = (a_1, b_2)$.

Finally, we recall from the proof of Theorem 3.1 that $z(x)$ is continuous on $[0, \infty)$, that $z(x) \to 0$ as $x \to \infty$, and $z(x) < 0$ for all large x. From this and property (A.24) it follows that there is a first $x_3 \in (x_1, \infty)$ such that $z(x_3) = 0$. That is,

$$2W(a_1 + x_3) + W(-x_3) - W(2a_1 + x_3) = 0. \tag{A.27}$$

Setting $b_3 = a_1 + x_3$, we write (A.27) as

$$2W(b_3) + W(a_1 - b_3) - W(a_1 + b_3) = 0. \tag{A.28}$$

Thus (3.3) is satisfied when $(a, b) = (a_1, b_3)$. This completes the proof of part (i).

Part (ii). It follows from the definition of $W(x)$ that (3.4) can be written as

$$h_i = -\int_0^{a_1} w(t)\, dt - \int_{b_i}^{a_1 + b_i} w(t)\, dt, \;\; i = 1, 2, 3. \tag{A.29}$$

To show that each h_i is negative requires that we consider two possibilities for b_i.

Case (I) $b_i \geq s_2$

Our hypotheses imply that (see Figure A.7)

$$\int_0^{a_1} w(t)\, dt = \int_0^{s_1} w(t)\, dt + \int_{s_1}^{a} w(t)\, dt > \int_0^{s_2} w(t)\, dt, \tag{A.30}$$

since $a_1 \in (s_1, s_2)$ and $w(x) < 0$ on (s_1, s_2).

Because $b_i \geq s_2$, we also obtain

$$\int_{b_i}^{a_1+b_i} w(t)\,dt > \int_{s_3}^{\infty} w(t)\,dt, \tag{A.31}$$

since $w > 0$ on (s_2, s_3) and $w < 0$ on (s_3, ∞). Substituting (A.30) and (A.31) into (A.29), and invoking (H_9), we conclude that

$$h_i < -\int_0^{s_2} w(t)\,dt - \int_{s_3}^{\infty} w(t)\,dt = -W(s_2) + W(s_3) - W(\infty) < 0, \tag{A.32}$$

as claimed.

Case (II) $b_i < s_2$

Here there are two subcases to consider. First, suppose that $a_1 + b_i \leq s_2$. Then $w(x) < 0$ on $(a_1, a_1 + b_i)$ and it follows that

$$\int_0^{a_1} w(t)\,dt + \int_{b_i}^{a_1+b_i} w(t)\,dt > \int_0^{s_2} w(t)\,dt. \tag{A.33}$$

Combining (A.33) with (A.29), we obtain

$$h_i = -\left(\int_0^{a_1} w(t)\,dt + \int_{b_i}^{a_1+b_i} w(t)\,dt\right) < -\int_0^{s_2} w(t)\,dt. \tag{A.34}$$

Thus, from (A.34) and (H_9) we obtain

$$h_i < -\int_0^{s_2} w(t)\,dt = -W(s_2) < W(\infty) - W(s_3). \tag{A.35}$$

But $W(\infty) - W(s_3) = \int_{s_3}^{\infty} w(t)\,dt < 0$ since $w(x) < 0$ for $x > s_3$. Thus $h_i < 0$ when $a_1 + b_i \leq s_2$. It remains to consider the possibility that $b_i < s_2 < a_1 + b_i$. In this case (A.29) becomes

$$h_i = -\left(\int_0^{a_1} w(t)\,dt + \int_{b_i}^{s_2} w(t)\,dt\right) - \int_{s_2}^{a_1+b_i} w(t)\,dt. \tag{A.36}$$

Note that

$$\int_0^{a_1} w(t)\,dt + \int_{b_i}^{s_2} w(t)\,dt > \int_0^{s_2} w(t)\,dt \tag{A.37}$$

since $w < 0$ on (b_i, s_2). Also,

$$\int_{s_2}^{a_1+b_i} w(t)\,dt > \int_{s_3}^{\infty} w(t)\,dt \tag{A.38}$$

since $w > 0$ on (s_2, s_3) and $w < 0$ on (s_3, ∞). Substituting (A.37) and (A.38) into (A.36), we once again obtain (A.32), hence $h_i < 0$ as required.

Part (*iii*). We recall from the stability analysis in Section 4 that the solution corresponding to $(a, b) = (a_1, b_1)$ is stable if the trace and determinant of the associated Jacobian matrix J defined in (4.18) have the correct signs. The trace and determinant are given by (4.24) and (4.25), respectively, where $(a, b) = (a_1, b_1)$. It follows from (5.4) and our hypotheses on w that

$$w(a_1) < 0 < w(b_1),\ \ w(b_1 - a_1) < 0 \ \text{ and } \ w(a_1 + b_1) < 0. \tag{A.39}$$

Using the inequalities in (A.39), we conclude that the trace is negative and the determinant is positive. From this it follows that both eigenvalues of the Jacobian matrix have negative real parts and therefore the solution is stable with respect to perturbations that do not break the equal–width condition. This completes the proof of the theorem.

A.3 Proof of Theorem 5.2

First, since a_1, b_1 and c_1 are given by (5.6), then

$$a_1 = (s_1 + s_2)/2, b_1 = 2a_1 = s_1 + s_2, \quad \text{and}\, c_1 = b_1 + a_1 = 3(s_1 + s_2)/2. \tag{A.40}$$

Furthermore, (H_{10}) implies that

$$s_1 < (s_1 + s_2)/2 < s_2 < s_1 + s_2 < s_3 < 3(s_1 + s_2)/2. \tag{A.41}$$

Combining (A.40) and (A.41), we obtain (see Figure A.8)

$$s_1 < (s_1 + s_2)/2 = a_1 < s_2 < s_1 + s_2 = b_1 < s_3 < 3(s_1 + s_2)/2 = c_1, \tag{A.42}$$

and therefore the conditions in (5.4) are satisfied.

Next, we show that (3.3) holds. First, from (5.7) and (H_{11}) we conclude that

$$\int_{a_1}^{2a_1} w(t)\,dt = \int_{a_1}^{s_2} w(t)\,dt + \int_{s_2}^{2a_1} w(t)\,dt = -A_1 + A_2 = 0. \tag{A.43}$$

The definition of $W(x)$ implies that (A.43) is equivalent to

$$W(2a_1) - W(a_1) = 0. \tag{A.44}$$

Similarly, it follows that

$$\int_{2a_1}^{3a_1} w(t)\,dt = \int_{2a_1}^{s_3} w(t)\,dt + \int_{s_3}^{3a_1} w(t)\,dt = A_3 - A_4 = 0, \tag{A.45}$$

or equivalently,

$$W(3a_1) - W(2a_1) = 0. \tag{A.46}$$

Next, substitute $(a, b) = (a_1, b_1)$ into the expression on the left side of (3.3) and use the fact that W is odd, together with (A.40), (A.44), and (A.46) to obtain

$$2W(b_1) + W(a_1 - b_1) - W(a_1 + b_1) = 2W(2a_1) - W(a_1) - W(3a_1) = 0. \tag{A.47}$$

Thus, (A.47) shows that (3.3) is satisfied when $(a, b) = (a_1, b_1)$.

Finally, (A.42) shows that $s_1 < a_1 < s_2$, and our hypotheses imply that $w > 0$ on $(0, s_1)$ and $w < 0$ on (s_1, s_2). From these facts and (H_9) we conclude that

$$W(a_1) = \int_0^{a_1} w(t)\,dt > \int_0^{s_2} w(t)\,dt = W(s_2) > 0. \tag{A.48}$$

From (A.44) and (A.48) it now follows that

$$2W(a_1) - W(2a_1) = W(a_1) > 0, \tag{A.49}$$

and therefore (5.3) is satisfied. This completes the proof.

References

[1] S. Amari, *Dynamics of pattern formation in lateral-inhibition type neural fields.* Biol Cybern. **27** (1977), pp. 77-87.

[2] W. F. Asaad, G. Rainer, & E. K. Miller. *Task–Specific Neural Activity in the Primate Prefrontal Cortex.* J. Neurophysiol. **84** (2000), pp. 451-459.

[3] W. H. Bosking, Y. Zhang, B. Schofield & D. Fitzpatrick. *Orientation Selectivity and the Arrangement of Horizontal Connections in Tree Shrew Striate Cortex.* J. Neurosci. **17** (1997), pp. 2112-2127.

[4] P. C. Bressloff. *Traveling fronts and wave propagation failure in an inhomogeneous neural network.* Physica D **155** (2001), pp. 83-100.

[5] P. C. Bressloff. *Bloch Waves, Periodic Feature Maps, and Cortical Pattern Formation.* Phys. Rev. Lett. **89** (2002), 088101.

[6] P. C. Bressloff, J. D. Cowan, M. Golubitsky, P. J. Thomas & M. Wiener. *Geometric visual hallucinations, Euclidean symmetry and the functional architecture of striate cortex.* Phil. Trans. Roy. Soc. B **40** (2001), pp. 299-330.

[7] P. C. Bressloff, J. D. Cowan, M. Golubitsky, P. J. Thomas & M. Wiener. *What geometric visual hallucinations tell us about the visual cortex.* Neural Comput. **14** (2002), pp. 473-491.

[8] A. Compte, N. Brunel, P. Goldman-Rakic, & X.-J. Wang. *Synaptic mechanisms and network dynamics underlying spatial working memory in a cortical network model.* Cereb Cortex. **10** (2000), pp. 910-923.

[9] S. Coombes, G. L. Lord & M. R. Owen, *Waves and bumps in neuronal networks with axo-dendritic synaptic interactions.* Physica D, to appear (2003).

[10] D. Durstewitz, J. K. Seamans & T. J. Sejnowski. *Neurocomputational models of working memory.* Nat. Neurosci. **3** (2000), pp. 1184-1191.

[11] G. B. Ermentrout. *Neural networks as spatio-temporal pattern forming systems.* Rep. Prog. Phys. **61**(4) (1998), pp. 353-430.

[12] M. A. Giese. *Dynamic Neural Field Theory for Motion Perception.* Kluwer Academic Publishers, Boston, 1998.

[13] B. Gutkin, G. B. Ermentrout, & J. O'Sullivan. *Layer 3 patchy recurrent connections may determine the spatial organization of sustained activity in the primate frontal cortex.* Neurocomputing **32-33** (2000), pp. 391-400.

[14] B. S. Gutkin, C. R. Laing, C. C. Chow, G. B. Ermentrout, & C. R. Colby. *Turning on and off with excitation: the role of spike–timing asynchrony and synchrony in sustained neural activity.* J. Comput. Neurosci. **11**(2) (2001), pp. 121-134.

[15] D. Hansel & H. Sompolinsky. *Modeling feature selectivity in local cortical circuits.* In Methods in Neuronal Modeling, second edition, ed. C. Koch and I. Segev. MIT Press, 1998.

[16] K. Kishimoto & S. Amari. *Existence and stability of local excitations in homogeneous neural fields.* J. Math. Biol. **7** (1979), pp. 303-318.

[17] C. R. Laing & C. C. Chow. *Stationary bumps in networks of spiking neurons.* Neural Comp. **13** (7) (2001), pp. 1473-1494.

[18] C. R. Laing, W. C. Troy, B. Gutkin & G. B. Ermentrout. *Multiple bumps in a neuronal model of working memory.* SIAM J. Appl. Math. **63** (2002), pp. 62-97.

[19] J. B. Levitt, D. A. Lewis, T. Yoshioka & J. S. Lund. *Topography of pyramidal neuron intrinsic connections in macaque monkey prefrontal cortex (areas 9 and 46).* J. Comp. Neurol. **338** (1993), pp. 360-376.

[20] D. A. Lewis & S. A. Anderson. *The functional architecture of the prefrontal cortex and schizophrenia.* Psychol. Med. **25** (5) (1995), pp. 887-894.

[21] R. Malach, Y. Amir, M. Harel & A. Grinvald. *Relationship Between Intrinsic Connections and Functional Architecture Revealed by Optical Imaging and in vivo Targeted Biocytin Injections in Primate Striate Cortex.* Proc. Natl. Acad. Sci. **90** (1993), pp. 10469-10473.

[22] E. K. Miller, C. A. Erickson, & R. Desimone. *Neural Mechanisms of Visual Working Memory in Prefrontal Cortex of the Macaque.* J. Neurosci. **16** (16) (1996), pp. 5154-5167.

[23] A. Pouget & L. H. Snyder. *Computational approaches to sensorimotor transformations.* Nat. Neurosci. **3** (2000), pp. 1192-1198.

[24] G. Rainer, W. F. Asaad, & E. K. Miller *Memory fields of neurons in the primate prefrontal cortex.* Proc. Natl. Acad. Sci. U. S. A. **95** (1998), pp. 15008-15013.

[25] B. Roerig & B. Chen *Relationships of Local Inhibitory and Excitatory Circuits to Orientation Preference Maps in Ferret Visual Cortex.* Cereb. Cortex **12** (2002), pp. 187-198.

[26] S. M. Stringer, T. P. Trappenberg, E. T. Rolls & I. E. T. de Araujo. *Self-organizing continuous attractor networks and path integration: one-dimensional models of head direction cells.* Network – Comp Neural **13** (2002), pp. 217-242.

[27] J. G. Taylor *Neural bubble dynamics in two dimensions: foundations* Biol. Cyb. **80** (1999), pp. 393-409.

[28] E. Thelen, G. Schöner, C. Scheier & L. B. Smith. *The Dynamics of Embodiment: A Field Theory of Infant Perseverative Reaching.* Behavioral and Brain Sciences **24**(1), (2000). Available at http://www.cogsci.soton.ac.uk/bbs/Archive/bbs.thelen.html.

[29] X. J. Wang. *Synaptic reverberation underlying mnemonic persistent activity.* Trends Neurosci. **24**(8) (2001), pp. 455-463.

[30] H. Werner & T. Richter. *Circular stationary solutions in two-dimensional neural fields* Biol. Cyb. **85** (2001), pp. 211-117.

[31] H. R. Wilson & J. D. Cowan. *A mathematical theory of the functional dynamics of cortical and thalamic nervous tissue.* Kybernetic **13** (1973), pp. 55-80.

[32] K. Zhang. *Representation of spatial orientation by the intrinsic dynamics of the head–direction cell ensemble: a theory.* J. Neurosci. **16** (1996), pp. 2112-2126.

List of Figures

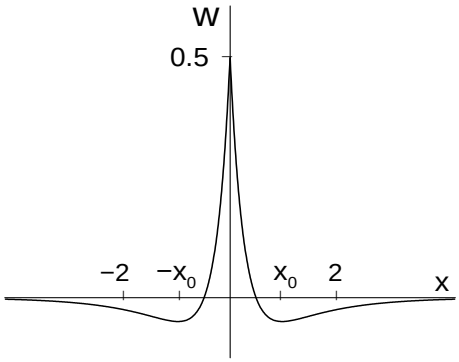

Fig. A.1. Mexican hat function (2.1) for parameters given in the text. The minimum for w occurs at $x_0 = 1.15$.

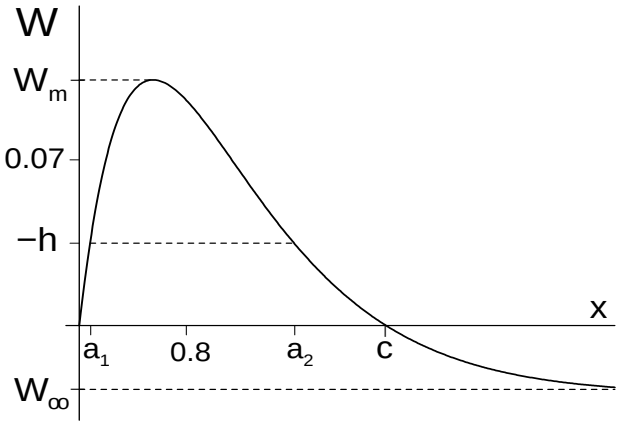

Fig. A.2. $W(x)$, (2.6), for the parameters in the text. We have chosen h to be negative, so that $W_\infty < 0 < -h < W_m$.

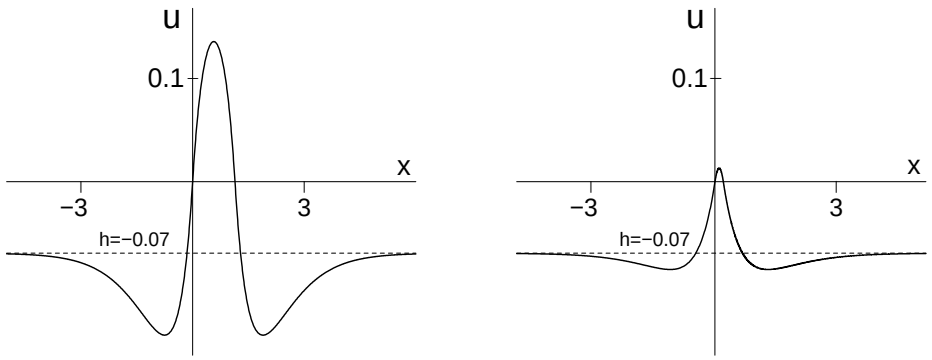

Fig. A.3. Stable (left) and unstable (right) single–bump solutions of (2.3) for the functions w and f shown in Figure A.1 and $h = -0.07$.

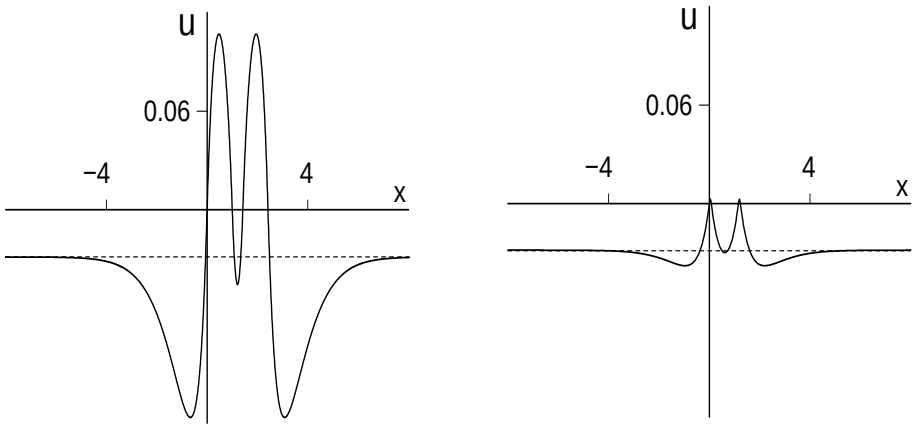

Fig. A.4. Two–bump solutions of (3.1) for $a = 1$ (left) and $a = 0.08$ (right). We have $h = -0.028$ for both solutions.

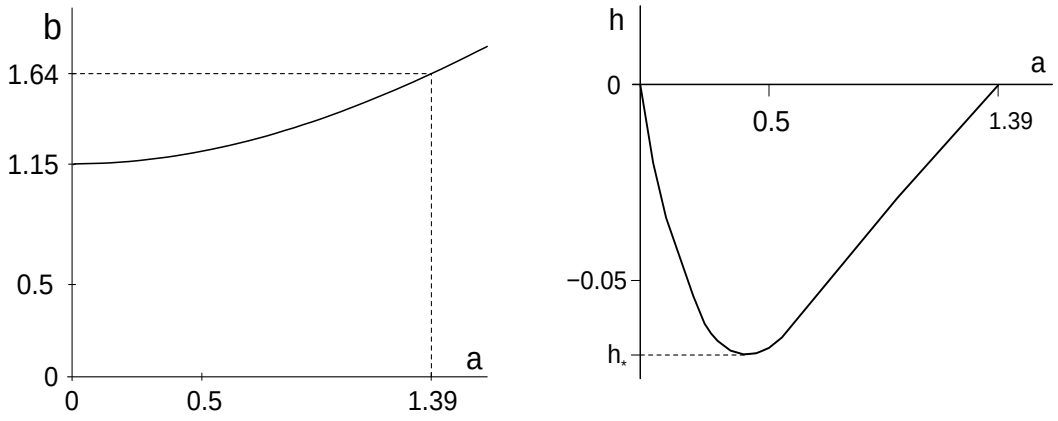

Fig. A.5. Left: b as a function of a from (3.3). Note that $b \to x_0$ as $a \to 0$, in accordance with (3.7) in Theorem 3.3. See also the rightmost (small a) solution in Figure A.4. Right: h as a function of a. If $h_* < h < 0$ then there are two values of a for which (3.1) has two–bump solutions.

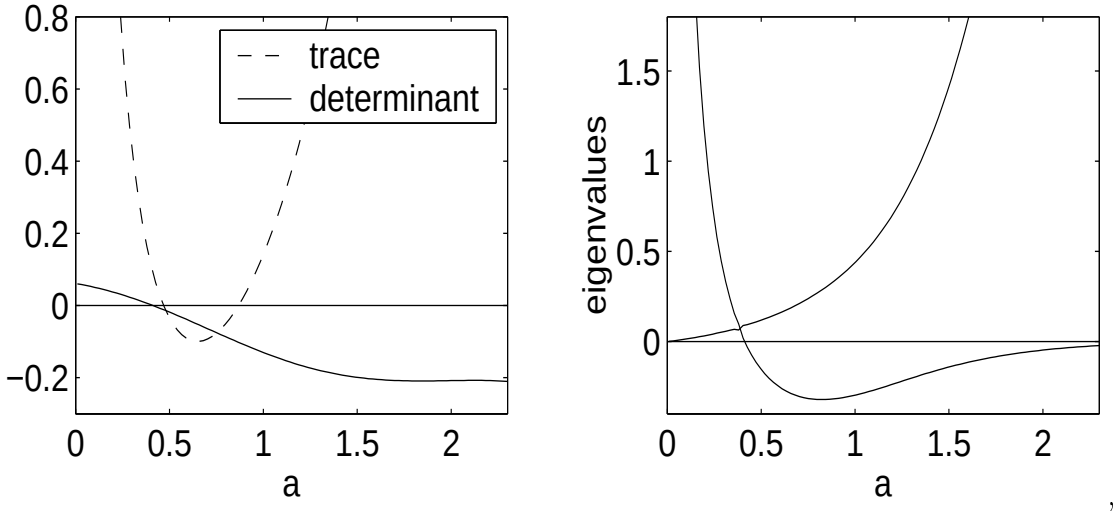

Fig. A.6. Left: trace (4.24) and determinant (4.25) as functions of a along the family of 2-bump solutions computed for the parameters $K = 3.5,\ k = 1.8,\ M = 3,\ m = 1.52$. Right: Corresponding eigenvalues (both real) as functions of a. For each a the solution is unstable since at least one eigenvalue is positive.

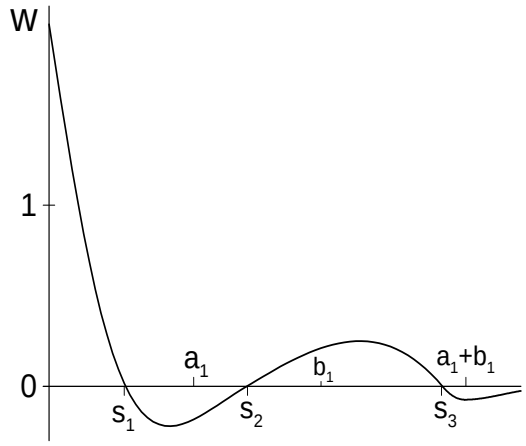

Fig. A.7. Coupling function satisfying $(H_1), (H_5), (H_7), (H_8), (H_9)$. Also, a_1, b_1 and $c_1 = a_1 + b_1$ satisfy condition (5.4) in Theorem 5.1.

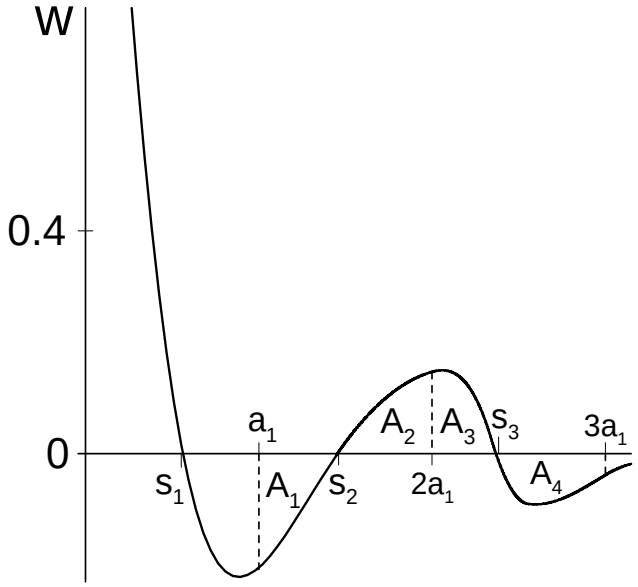

Fig. A.8. Coupling function satisfying hypotheses $(H_1), (H_5)$ and (H_7) – (H_{11}), and $a_1 = (s_1 + s_2)/2, b_1 = 2a_1$ and $c_1 = 3a_1$ satisfy conditions (5.3) and (5.4).

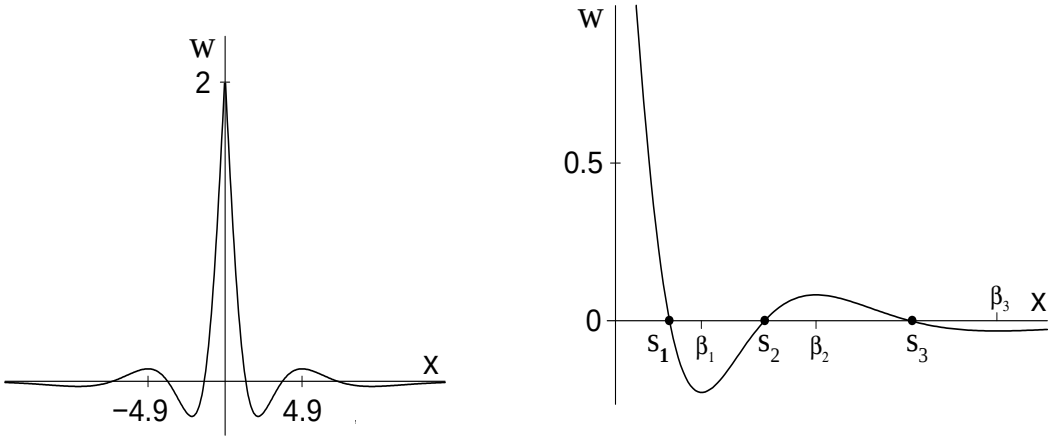

Fig. A.9. Left: The coupling function defined in (5.9) for parameter values given in (5.10). Compare with Figure A.1. Right: A blowup of the coupling function shown at left. $w = 0$ at $s_1 = 1.32,\ s_2 = 3.65,\ s_3 = 7.18$, and $w' = 0$ at $\beta_1 = 2.11,\ \beta_2 = 4.9$, and $\beta_3 = 9.32$. .

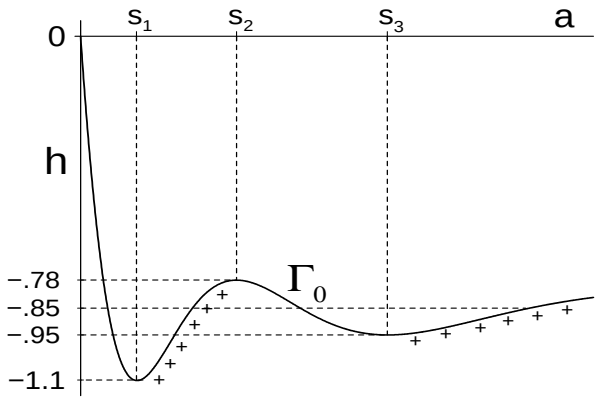

Fig. A.10. A plot of the function $h = -W(a)$ for the coupling given by (5.9)-(5.10). Along $\Gamma_0 = \{(a, h) | a > 0 \text{ and } h = -W(a)\}$ stable 1-bump solutions are indicated by plus signs. The maxima and minima are given by $s_1 = 1.32, s_2 = 3.65$ and $s_3 = 7.18$. Compare with Figure A.2.

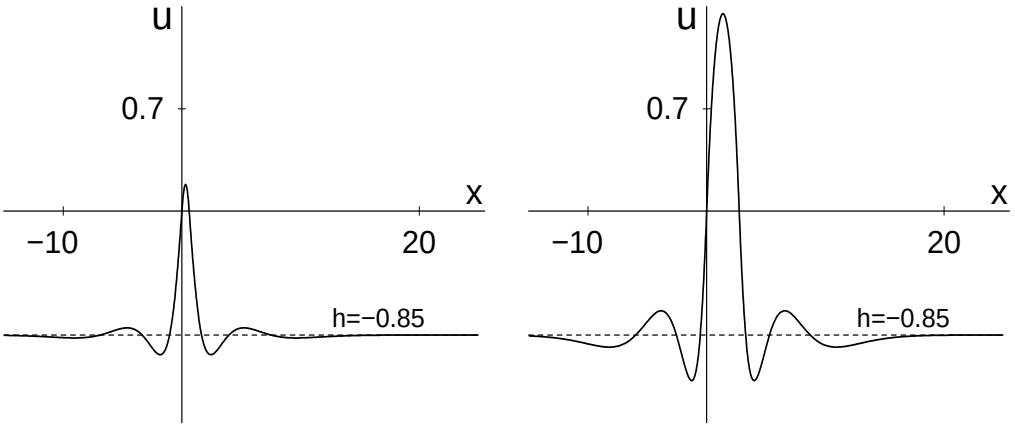

Fig. A.11. Unstable (left) and stable (right) 1–bump solutions of (5.8). The values of a are $a = 0.61$ (left) and $a = 2.73$ (right). These solutions are comparable to the 1–bump solutions shown in Figure A.3 for lateral inhibition couplings.

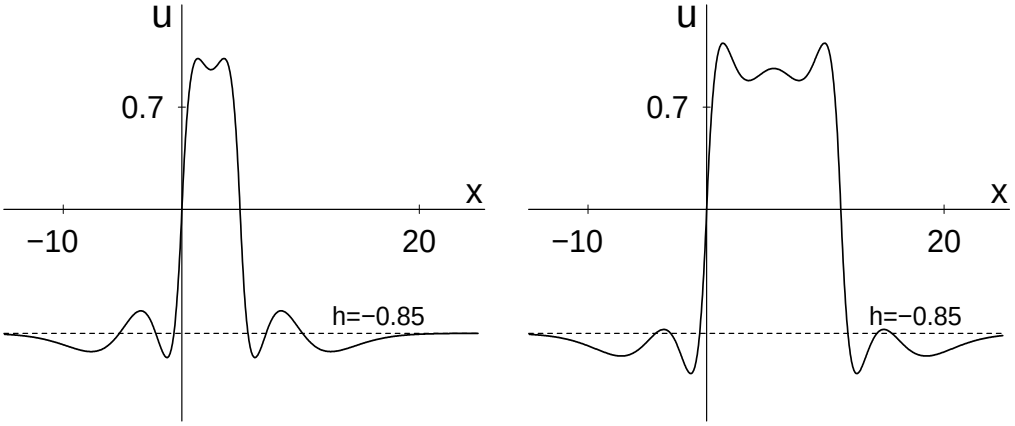

Fig. A.12. Unstable (left) and stable (right) 1–bump solutions of (5.8). The a values are $a = 4.89$ (left) and $a = 11.3$ (right).

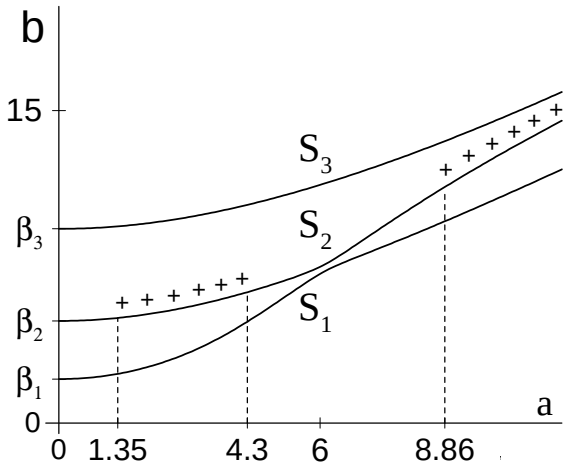

Fig. A.13. Three branches S_1, S_2 and S_3 of 2–bump solutions. Points on these curves satisfy (3.3). Stable solutions are indicated by plus signs on S_2. Along each S_i we find that $b(a) \to \beta_i$ as $a \to 0^+$, where $w'(\beta_i) = 0$. Compare with Figure A.5.

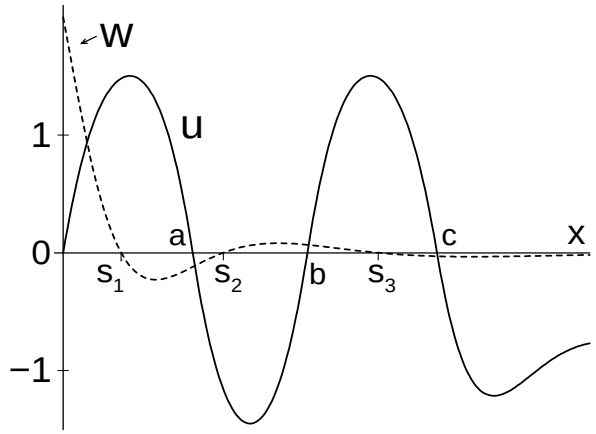

Fig. A.14. Stable 2–bump solution (solid curve) of (5.8) for parameters given in (5.10). Here $a = 2.95,\ b = 5.56,\ c = a + b = 8.51$ and $h = -0.85$. The dashed curve is the coupling defined in (5.9). The conditions for stability given in Theorem 5.1 are satisfied since $a \in (s_1, s_2),\ b \in (s_2, s_3)$ and $c \in (s_3, \infty)$.

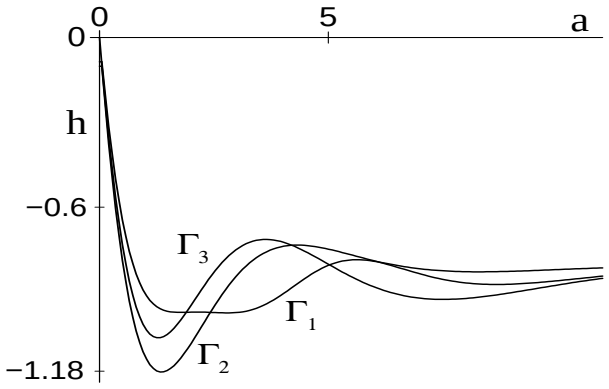

Fig. A.15. h as a function of a (using (3.3) and (3.4)) for 2–bump solutions. Each Γ_i corresponds to an S_i in Figure A.13. Compare with Figure A.5, right.

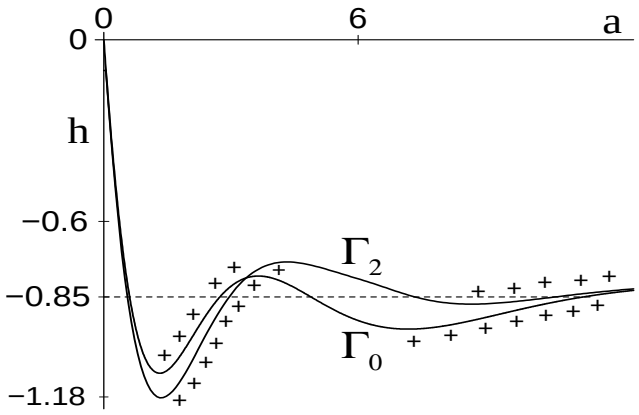

Fig. A.16. The curves Γ_0 (of 1–bump solutions) and Γ_2 (of 2–bump solutions) are shown in the (a, h) plane. Stable solutions are indicated by plus signs. If $-0.875 < h < -0.8$ then two stable 1–bump solutions and two stable 2–bump solutions coexist (along with two unstable 1–bump solutions and two unstable 2–bump solutions).

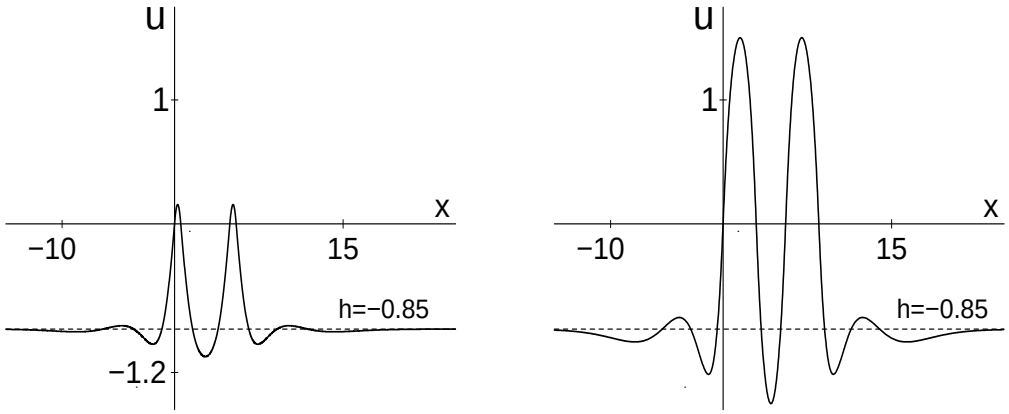

Fig. A.17. Unstable (left) and stable (right) 2–bump solutions of (5.8) for $h = -0.85$. The values of a are $a = 0.55$ (left) and $a = 2.95$ (right). The parameters for the coupling are given in (5.10). The shapes of these solutions are similar to the unstable 2–bump solutions found earlier for lateral inhibition coupling, shown in Figure A.4.

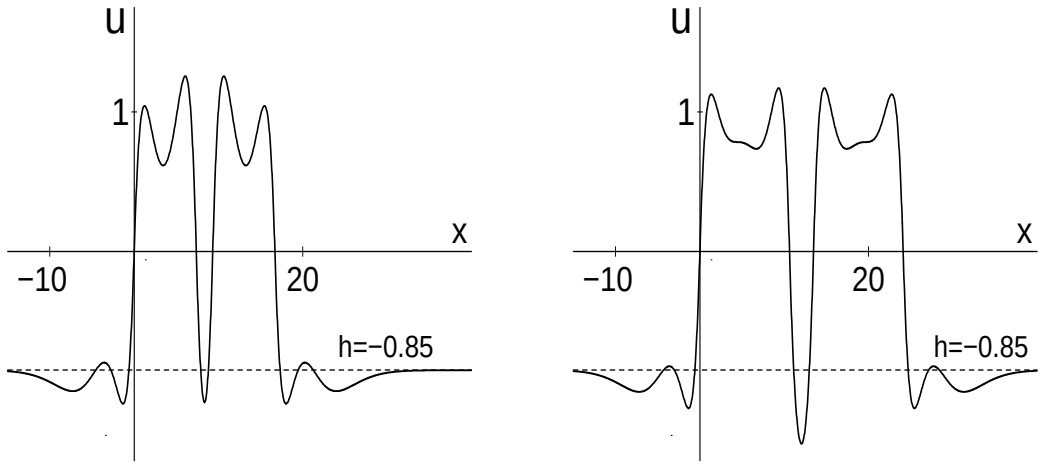

Fig. A.18. Unstable (left) and stable (right) 2–bump solutions of (5.8) for $h = -0.85$. The a values are $a = 7.36$ (left) and $a = 10.63$ (right).

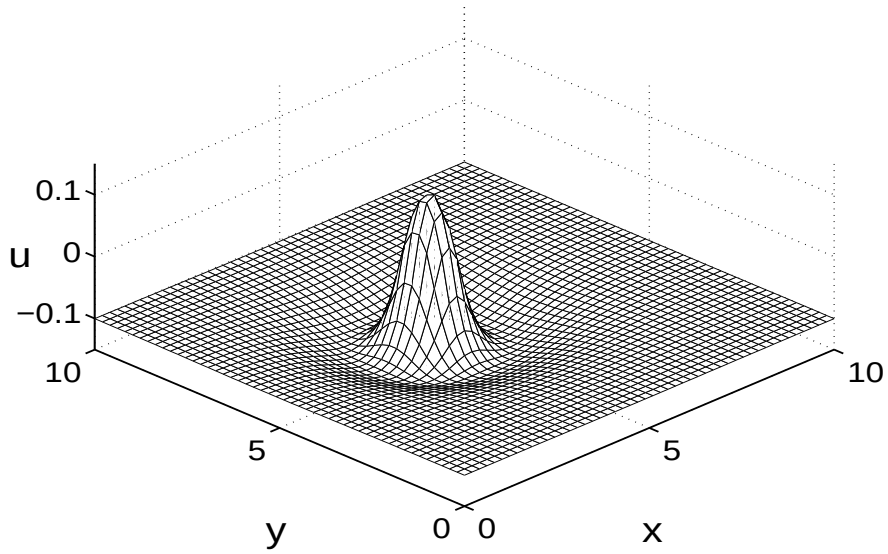

Fig. A.19. One–bump solution of (6.1)-(6.2). Parameters are $K = 3.5$, $k = 1.8$, $M = 2.8$, $m = 1.52$ and $h = -0.1$.

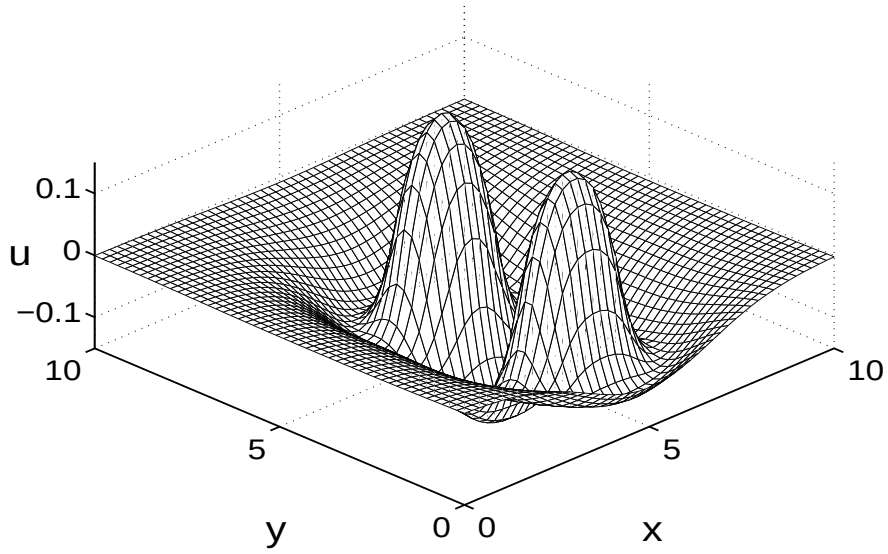

Fig. A.20. Two–bump solution of (6.1)-(6.2). Parameters are $K = 3.5$, $k = 1.8$, $M = 2.8$, $m = 1.52$ and $h = 0$.

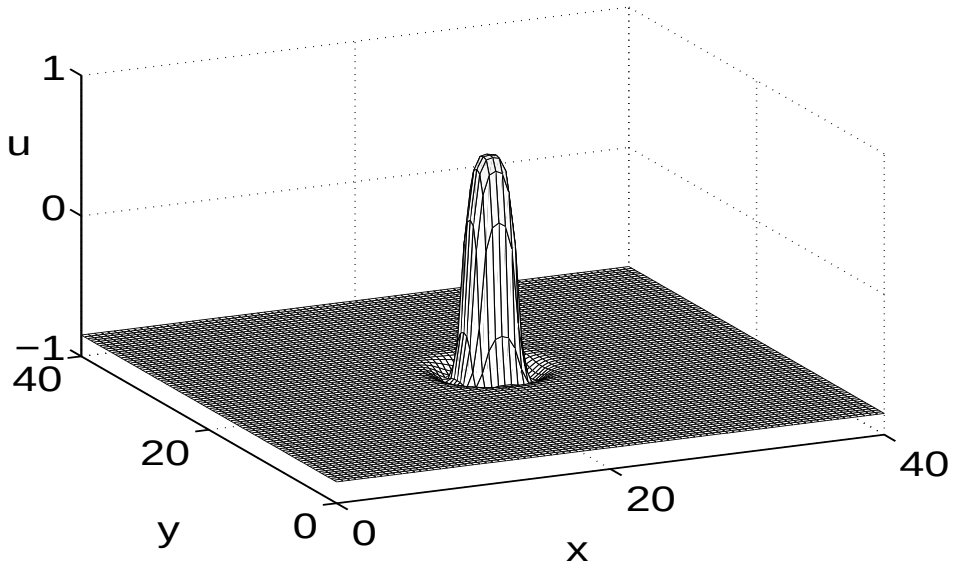

Fig. A.21. A 1–bump solution for the coupling given in (6.3)-(6.4). Here $h = -0.85$. Compare with the one–dimensional solution in Figure A.11, right panel.

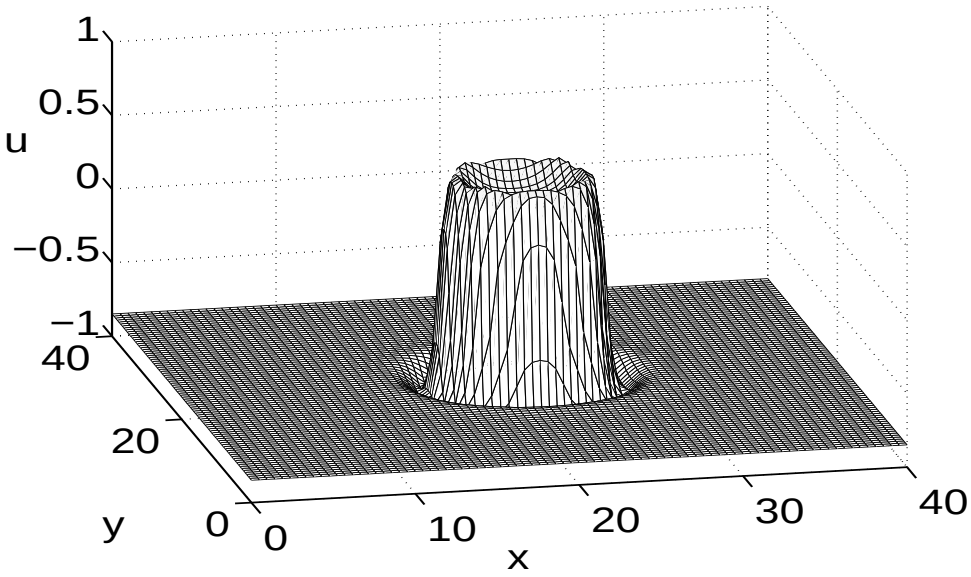

Fig. A.22. Second 1–bump solution for the coupling given in (6.3)-(6.4). Here $h = -0.85$. Compare with the one–dimensional solution in Figure A.12, right panel.

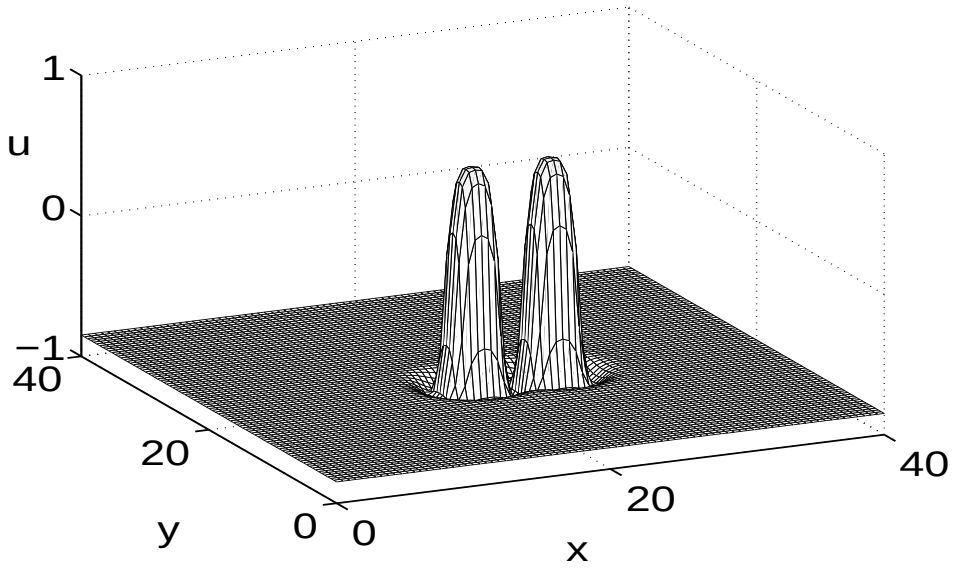

Fig. A.23. A 2–bump solution for the coupling given in (6.3)-(6.4). Here $h = -0.85$. Compare with the one–dimensional solution in Figure A.17, right panel.

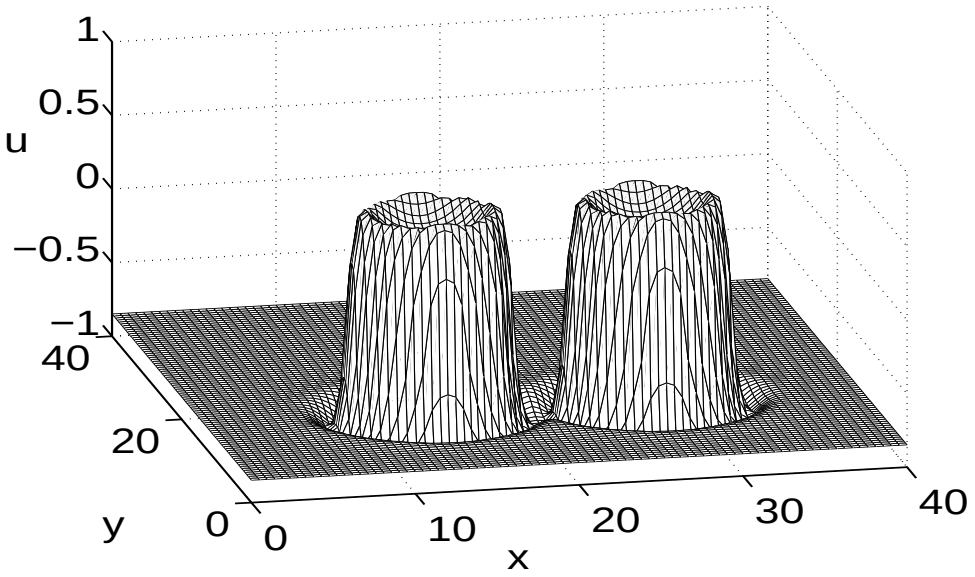

Fig. A.24. Second 2–bump solution for the coupling given in (6.3)-(6.4). Here $h = -0.85$. Compare with the one–dimensional solution in Figure A.18, right panel.